January 2018

Differential Gene Expression Of Muscle-Invasive Bladder Cancer Marker Genes In A Model Of Arsenite And Cadmium Induced Bladder Cancer

Danyelle Beth Osowski

[How does access to this work benefit you? Let us know!](#)

Follow this and additional works at: https://commons.und.edu/theses

DIFFERENTIAL GENE EXPRESSION OF MUSCLE-INVASIVE BLADDER
CANCER MARKER GENES IN A MODEL OF ARSENITE AND CADMIUM
INDUCED BLADDER CANCER

by

Danyelle Beth Osowski

Bachelor of Science, University of North Dakota, 2016

A Thesis

Submitted to the Graduate Faculty

of the

University of North Dakota

in partial fulfillment of the requirements

for the degree of

Master of Science

Grand Forks, North Dakota
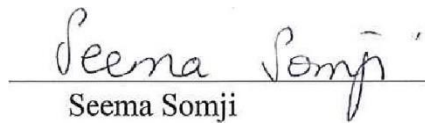
December
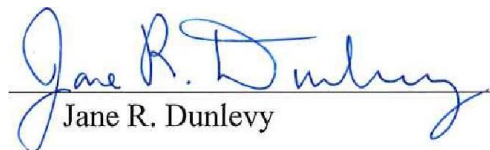
2018
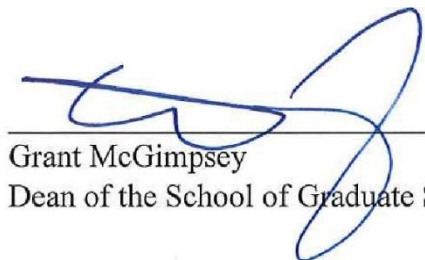
This thesis, submitted by Danyelle Beth Osowski in partial fulfillment of the requirements for the Degree of Master of Science from the University of North Dakota, has been read by the Faculty Advisory Committee under whom the work has been done and is hereby approved.

_____
Scott H. Garrett

_____
Seema Somji

_____
Jane R. Dunlevy

This thesis is being submitted by the appointed advisory committee as having met all of the requirements of the School of Graduate Studies at the University of North Dakota and is hereby approved.

_____
Grant McGimpsey
Dean of the School of Graduate Studies

December 5, 2018
_____
Date

PERMISSION

Title   Differential Gene Expression of Muscle-Invasive Bladder Cancer Marker
             Genes in a Model of Arsenite and Cadmium Induced Bladder Cancer

Department   Pathology

Degree   Master of Science

        In presenting this thesis in partial fulfillment of the requirements for a graduate
degree from the University of North Dakota, I agree that the library of this University
shall make it freely available for inspection. I further agree that permission for extensive
copying for scholarly purposes may be granted by the professor who supervised my
thesis work or, in his absence, by the Chairperson of the department or the dean of the
School of Graduate Studies. It is understood that any copying or publication or other use
of this thesis or part thereof for financial gain shall not be allowed without my written
permission. It is also understood that due recognition shall by given to me and the
University of North Dakota in any scholarly use in which may be made of any material in
my thesis.

                                            Danyelle Beth Osowski
                                            December 5, 2018

TABLE OF CONTENTS

vi

LIST OF FIGURES

LIST OF TABLES

ACKNOWLEDGEMENTS

Dedicated to the memory of my grandpa, Eddie, who always believed in my ability to be successful in the academic arena. You are gone, but your belief in me has made this journey possible.

ABSTRACT

Urinary carcinoma is one of the most prevalent cancers across the United States

and is among the leading cause of cancer related morbidities. With muscle-invasive

urinary carcinoma having only 15% survival at stage T4, diagnostic tools of this type of

cancer is necessary. This work sought to characterize a model of urothelial carcinoma

into a specific muscle-invasive bladder cancer subtype, which has important implications

in for prognosis, development of targeted therapeutic agents, and disease management.

Our laboratory has developed an immortalized uroepithelial cell line, UROtsa, which can

be malignantly transformed by arsenite (As^{+3}) and Cd^{2+} and has been shown to produce

colonies on soft agar and tumors in nude mice. We therefore sought to determine if which

subtype of muscle-invasive bladder cancer in our six As^{3+} and seven Cd^{2+}-transformed

cell lines and heterotransplant tumors. Real-time reverse transcriptase polymerase chain

reaction (RT-PCR) was used to determine mRNA levels of 25 marker genes of basal and

luminal subtypes of muscle-invasive bladder cancer. Western blotting and

immunohistocemical analysis of select markers was used to evaluate protein expression.

Data indicated that the expression of the 25 marker genes in the As^{3+} and Cd^{2+}-

transformed tumors was increased in the basal subtype compared to the luminal subtype.

This same expression pattern was also seen in the transformed As^{3+} and Cd^{2+} cell lines

and spheroids, or putative cancer stem cells, derived from our transformed cell lines via

culture in serum-free media in low attachment flasks. Next, we sought to determine the

mRNA and protein expression in our non-tumorigenic parental UROtsa cell line. We

determined the parental UROtsa cell line had increased expression of the basal marker

xiii

genes and this was further increased in the spheroids, while expression of the luminal

marker genes was seen to be further decreased in expression in the spheroids.

Due to the observations seen in the mRNA expression of the spheroids, we

became interested in the ability of these cells to maintain their gene signature when

replaced back into the cell culture conditions of the original cell line. To do this, one As^{3+}

cell line was grown in serum media and cell culture flasks that promote attachment. From

there, the cells were placed into low attachments flasks with serum-free media to produce

spheroids. Once grown, the cells were reintroduced into cell culture flasks that promote

cell attachment with serum-containing media and harvested once reaching confluency

(P1) and passages 4 and 8 (P4 and P8). Microarray analysis of these samples found that

there were 4,415 differentially expressed genes when comparing the original cell line to

the spheroid. This number decreased at each comparison of the passages to the cell line

with 1,290, 452, and 191 differentially expressed genes compared to the cell line at P1,

P4, and P8 respectively. This data indicated that the replacement of our spheroids into

cell culture conditions identical to the original cell line promoted the reversal of the

spheroids into our original cell line cultures. We next sought to understand if the gene

signature of the spheroids would be maintained if they were cultured in conditions of

flasks that promote cell attachment with serum-free media in the same As3+ transformed

cell line, but also a Cd2+ cell line and our original parental UROtsa cell line. By

performing real-time RT-PCR analysis of the 25 muscle-invasive bladder cancer marker

genes, we found the number of differentially expressed genes compared to the cell line

and either the spheroid or subsequent passages was relatively stable with at least 68% of

the genes being differentially expressed by P8. This data demonstrates we have a unique

gene signature that does not align with the original cell line.

CHAPTER I

INTRODUCTION

Urinary Carcinoma

Urinary carcinoma accounts for a significant number of cancer morbidity and mortality with an estimated 430,000 new cases diagnosed in 2012 (Antoni, et al., 2016) and 115,000 deaths each year (Meliker & Nriagu, 2007). Incidence rates are 3 to 4 times higher in men than in women and the disease prevalence increases with age; 80% of cases in occur in patients ages 50 to 79 (Wai & Miller, 2002). Despite this type of cancer being only the fourth most common in males and ninth most common in females (Crawford, 2008), it is the most expensive cancer from diagnosis to death with the annual cost in 2013 being $US4.25 billion (Yeung, Dinh, & Lee, 2014).

Urinary carcinoma typically arises from the transitional cells of the bladder, termed the urothelium, and accounts for 95% of all diagnosed cases (Malats & Real, 2015). These tumors can be of two types: a low-grade, non-invasive tumor, which occurs 70% of the time with high rates of recurrence, but infrequently progresses to muscle invasion or an aggressive, muscle-invasive disease with 5-year survival rates of less than 50% (Yousef & Gabril, 2017).

Anatomy of the Urinary Bladder

The urinary bladder is a muscular organ that functions to collect and store urine before it is excreted from the body. As mentioned above, the bladder consists of specialized epithelial cells called the urothelium, which has properties to allow for filling and voiding

in at least two ways. First, the bladder, much like the stomach, is highly wrinkled, which allows for the storage of urine by unfolding of the walls of the bladder. Secondly, during filling, the urothelium becomes thinner due to a change in the morphology of the cells that it is comprised of (Apodaca, 2004). Three types of cells coat the surface of the urothelium: umbrella, intermediate, and basal cells. The outermost cells are the umbrella cells that are unique to the urothelium and which form a barrier that functions to prevent the entry of pathogens and controls the intake of molecules into the underlying tissues layers. Sitting just below the umbrella cells are the intermediate cells that may be one to several layers thick and are rapidly regenerated. The bottom-most layer of the urothelium is comprised of the basal cells, which form a single layer that is in contact with the connective tissue below. These cells have a low mitotic index and contain the urothelial stem cells, which play a critical role in regeneration.

The sub-urothelium or lamina propria is comprised of an extracellular matrix, which contains fibroblasts, adipocytes, nerve endings, blood vessels, and the muscularis mucosae muscle layer. Deep to this layer is the detrusor layer that contains three layers of smooth muscle bundles of the detrusor muscle (inner longitudinal, middle circular, and outer longitudinal) along with connective tissue and interstitial cells. This muscle of the bladder is covered by a thin membranous connective tissue termed the external serosa and is surrounded by perivesical fat in the abdominal cavity.

Signs and Symptoms of Urinary Carcinoma

The most common symptom of urinary carcinoma is gross painless hematuria, also known as the presence of blood in the urine. This symptom presents itself in 85% of patients at initial diagnosis (Alishahi, Dyrne, Goodman, M., & Baxby, 2002). The second

most common symptom is asymptomatic microscopic hematuria with up to 10% of patients

diagnosed with urinary carcinoma (Metts, Metts, Milito, & Thomas Jr., 2000). A study of

1,046 patients, 657 and 389 presenting with microscopic and gross hematuria respectively,

found that 25% of those presenting with gross hematuria had a urological malignancy

compared to only 3.7% of patients with microscopic hematuria (Alishahi, Dyrne,

Goodman, M., & Baxby, 2002). In addition, of the 1,930 patients enrolled in a study at a

hematuria clinic, 12% were found to have urinary carcinoma (Khadra, Pickard, Charlton,

Powell, & Neal, 2000). The remaining patients that do not present with the symptoms

mentioned above do present with signs that mimic other common urological diseases, such

as urinary tract infections.

<div align="center">Muscle-Invasive Urinary Carcinoma</div>

At the time of diagnosis, approximately one-third of urinary tumors present as non-

papillary lesions and have a high propensity for metastasis (Malkowicz, et al., 2007). These

tumors consist of those staged from T_2 to T_4. These high-grade tumors have overall 5-year

survival rates of 68% for patients with a T_2 diagnosis to only 15% for those with T_4

(Goebell & Knowles, 2010). The invasion of a tumor into the muscularis propria is staged

as T_2, while stages T_3 and T_4 are characterized by the invasion of the perivesical soft tissue

or invasion into an adjacent organ, which include the vagina, uterus, prostate, pelvic wall

or abdominal wall, respectively (Cheng, Montironi, Davidson, & Lopez-Beltran, 2009).

With evidence supporting differences in morphology and survival rates, it is hypothesized

that there are separate oncogenic pathways for non-invasive and muscle-invasive tumors.

Animal studies have proposed the expression of the SV40 large T antigen to inactivate the tumor protein p53 (TP53) and retinoblastoma (RB) pathways to induce non-papillary, invasive urinary carcinoma (Zhang, Pak, Shapiro, Sun, & Wu, 1999). The p53 family of transcription factors functions to regulate vital cell processes, which include differentiation, proliferation, and control over cell death and survival (Kaghad, et al., 1997). The RB1 protein is a negative regulator of the cell cycle by controlling progression through the G1 phase (Goodrich, Wang, Yue-Wei, Lee, & Lee, 1991). Inactivation of both TP53 and RB proteins leads to loss of cell cycle control, which in turn affects many aspects of tumorigenesis, such as differentiation, survival, senescence, and genomic stability.
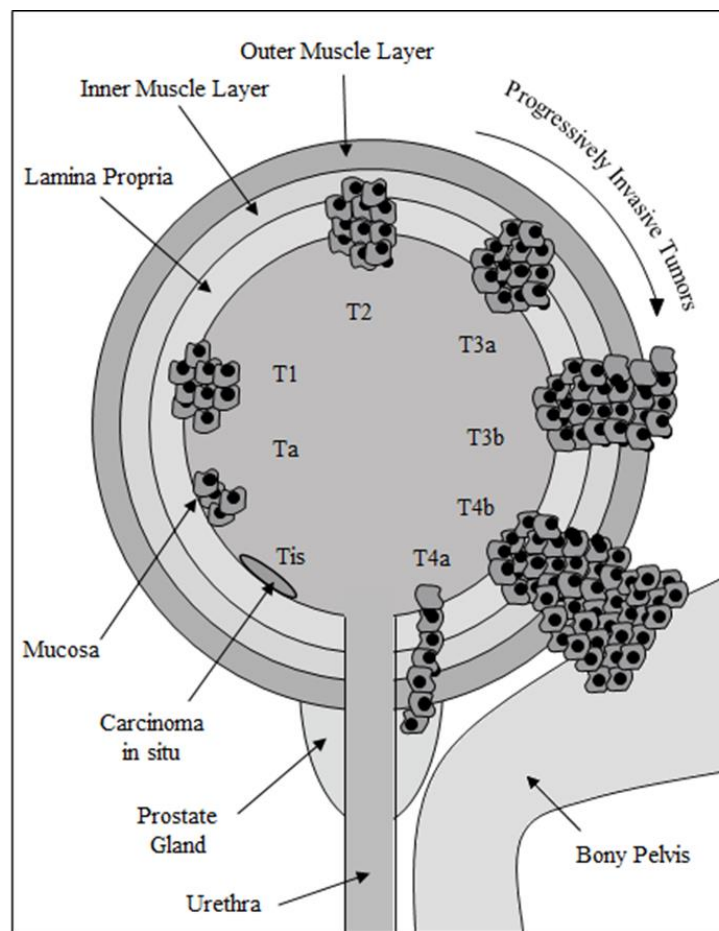
Figure 1. Urinary carcinoma staging according to the TMN system (Adapted from van der Meijden A. P., 1998).

Another frequently found mutation in invasive bladder tumors is phosphatidylinositol (3,4,5)-trisphosphate [PtdIns(3,4,5)P3] phosphatase and tensin homolog (PTEN). PTEN is involved in the conversion of lipid second messengers, which antagonizes signaling cascades downstream of receptor tyrosine kinases (RTKs) and phosphatidylinositol-3-kinase (PI3K) (Maehama & Dixon, 1998). The inactivation of PTEN leads to the dysregulation of the mammalian target of rapamycin pathway (mTOR), which in turn inhibits its blocking of bladder tumors (Puzio-Kuter, et al., 2009).

Diagnosis of Muscle Invasive Urinary Carcinoma

Muscle-invasive tumors are diagnosed after further investigation into the cause of hematuria. While urine cytology studies have poor sensitivity in detecting low-grade cancers (Badalament, Fair, Whitemore Jr., & Melamed, 1988), they are highly predictive of high-grade cancers (Droller M. J., 1998). Recently, there have been proposed markers in voided urine that may help in the detection of bladder cancer. A promising assay, the bladder tumor antigen (BTA) test, detects the release of extracellular matrix proteins from urinary carcinoma (Sarodsy, et al., 1997). However, specificity of high-grade carcinomas may be affected by infections of the urinary tract, the presence of stones, and other causes of inflammation, which deems this assay unreliable for cancer detection (Droller M. J., 1998). A second molecule being tested for its potential as a diagnostic tool for urinary carcinoma is telomerase, a ribonucleoprotien enzyme that functions to produce telomeres (Lin, et al., 1996). Detection of telomerase levels in voided urine have been found to have a sensitivity of 87.5% for high-grade tumors and an overall specificity of 70% for both low- and high-grade tumors (Kavaler, Landman, Y, Droller, & Liu, 1998).

Treatment of Muscle Invasive Urinary Carcinoma

Along the same ideals as low-grade tumors, the standard treatment for muscle invasive urinary carcinoma is radical cystectomy with lymph node dissection (Sridhar, 2017). This procedure is not without drawbacks; in up to as much as 64% of patients, radical cystectomy leads to peri- and postoperative complications within the first three months post-surgery (Donat, et al., 2009) and failure occurs in 70% to 80% of patients with aggressive disease (Skinner & Lieskovsky, 1984).

With the global life expectancy increasing yearly, there will be a larger population of patients with bladder cancer who have an advanced disease and radical cystectomy will no longer be a viable option for treatment. A study found that 25% of patients ages 70-79 and 40% of patient's ages 80-89 were treated with observation alone (Gray, et al., 2013). In addition, younger patients who wish to avoid the complications associated with radical cystectomy may be candidates for other types of treatments, which include partial cystectomy, transurethral resection of the bladder tumor (TURBT), chemotherapy and radiation therapy.

In order to give patients a better chance of survival and remission, neoadjuvant and perioperative chemotherapies have been developed. For neoadjuvant chemotherapy, cisplatin-based is recommended by both the North American and European guidelines (Clark, et al., 2016) (Witjes, et al., 2016). Different combinations of drugs have been tested and common regimens include methotrexate, vinblastine, doxorubicin, and cyclophosphamide (MVAC) and gemcitabine plus cisplatin (GC) (Galsky, et al., 2015). For those who are unfit for cisplatin-based therapy and those who fail to respond to such treatment, other options have been explored, such as carboplatin-based drug combinations

that have resulted in overall survival rates of 9 months (De Santis, et al., 2012). By instilling this multidisciplinary approach to treating urinary carcinoma, hopefully more patients will have an easier time managing their disease, a better quality of life, and have more positive outcomes.

The need for more therapy options for bladder tumors and the investigation of immunotherapies for other types of cancers has led to the development of drugs as new treatment tools. One therapeutic avenue that has emerged as a promising target is the programmed cell death protein 1 (PD-1) and programmed death ligand 1/2 (PD-L1/2) pathway. Under homeostatic conditions, PD-1 functions to regulate T cell responses by interacting with PD-L/1/2. However, in urinary carcinoma, PD-1 and PD-L1 are upregulated, which through their interaction promotes T-cell exhaustion (Tumeh, et al., 2014). By blocking the interaction with the PD-1 receptor with antibodies, there is a restoration of T-cell function (Chism, 2017).

Molecular Subtypes of Muscle-Invasive Urinary Carcinoma

Understanding the molecular expression patterns of heterogeneous tumors could lead to improved therapeutic strategies by finding new molecules to target and give insight into how individual tumors will respond to therapies. This was first accomplished by analyzing gene expression patterns in normal and malignant breast cancer tissue along with cell lines and clustering all the samples according to their patterns of expression. The study found four groups of samples that had different molecular features and were named ER+/luminal-like, basal-like, *Erb-B(II)* and normal (Perou, et al., 2000). This same idea has been used to understand the phenotypic diversity of many types of cancer including urinary carcinoma.

An investigative group from the University of North Carolina at Chapel Hill sought to understand the intrinsic molecular subtypes of high-grade bladder carcinoma. By analyzing 262 high-grade muscle-invasive tumors from public datasets and 49 high-grade tumors, they found two groups, named K1 and K2, which had different gene expression signatures. Clustering of the K1 data set found high levels of the high molecular weight keratins, specifically keratin 14 (KRT14), keratin 5 (KRT5), and keratin 6B (KRT6B), along with the cluster of differentiation molecule 44 (CD44). Conversely, the K2 cluster expressed high levels of uroplakins, specifically uroplakin 1B (UPK1B), uroplakin 2 (UPK2), and uroplakin 3 (UPK3), and the low molecular weight keratin, keratin 20 (KRT20). Furthermore, they performed ingenuity pathway analysis (IPA) and found the tumors in the K1 cluster were associated with carcinogenesis and cell survival and movement (Damrauer, et al., 2014).

A second group from Lund University in Sweden analyzed 144 urinary carcinomas by whole genome array-comparative genomic hybridization and mutational analysis of genes known to be implicated in the development of urinary tumors. Their clustering results found two intrinsic molecular subtypes, which they proceeded to name MS1 and MS2. Further analysis of the two groups found distinct enrichment of genes between the subtypes with cell cycle genes, cellular transformation, and genomic instability in the MS2 subtype. Taken together, these particular gene enrichments suggest the MS2 subtype to be more aggressive than MS1. The mutational analysis found distinct patterns for mutations in the genes implicated in the two hypothesized pathways of the development of urinary carcinoma. Activating mutations in fibroblast growth factor receptor 3 (FGFR3)/ phosphatidylinositol-4,5-bisphosphate 3-kinase catalytic subunit alpha (PIK3CA) were

found in the MS1 tumors, while alterations in TP53/ MDM2 proto-oncogene (MDM2) and

a loss of RB1 were significant in MS2 tumors (Lindgren, et al., 2010).

A follow-up study by this group extended their previous research and found 5 major

subtypes of urinary carcinoma: urobasal A, urobasal B, genomically unstable, squamous-

cell carcinoma (SCC) like, and a heterogeneous, infiltrated group. The urobasal A tumors

had elevated expression levels of FGFR3, cyclin D1 (CCND1), and tumor protein 63

(TP63) and showed a good prognosis. The genomically unstable tumors were characterized

by TP53 mutations and genes found to be associated with tumor progression and

recurrence, such as karyopherin subunit alpha 2 (KPNA2) and heme oxygenase 1

(HMOX1) (Staack, et al., 2002). High expression of the basal keratins KRT4, KRT6A,

KRT6B, KRT6C, KRT14, and KRT16 were found in the SCC-like tumors. The urobasal

B tumors were enriched in FGFR3 mutations along with FGFR3, CCND1, and TP63 gene

expression, similar to the urobasal A subtype. However, this group showed expression of

some keratins of the SCC-like group and TP63 mutations, which led researchers to believe

this group is more progressed than the urobasal A group. Finally, the infiltrated tumor

group was characterized by the presence of immunologic and myofibroblast cells (Sjödahl,

et al., 2012).

The final investigative team to pioneer this research in urinary carcinoma out of the

University of Texas MD Anderson Cancer Center performed whole genome mRNA

expression profile on 73 TURBT muscle-invasive samples. By doing this they identified

three distinct subtypes: basal, luminal, and p53-like. The basal tumors were characterized

by upregulated gene expression of CD44, KRT5, KRT6, KRT16, and CDH3 and was

associated with shorter overall survival and disease-specific survival. On the other hand,

luminal tumors were enriched in high expression and mutations of FGFR3. The transcription factors peroxisome proliferator activator receptor gamma (PPARγ) and its coactivator fatty acid binding protein 4 (FABP4) were also found to be strongly expressed in luminal tumors (Choi, et al., 2014).

Taken altogether, more aggressive tumors in the above studies, namely basal, were characterized by areas of squamous differentiation and high expression of high molecular weight keratins (KRT5, KRT6, KRT14, and KRT16) along with CDH3 and CD44. These tumors were found to have mutations in RB1 and were associated with shorter overall disease-specific survival and carcinogenesis. In contrast, tumors that were found to be less aggressive, or luminal, were characterized by mutations in FGFR3 and high expression levels of uroplakins and KRT20 along with the transcription factors PPARγ and FABP4.

Tumor-Derived Spheroids as an *In Vitro* Model System

Two-dimensional (2D) monolayer cell cultures are an indispensable tool that allows researchers to understand many functions and characteristics of tissue samples, as well as an excellent model to test new therapeutics without using animals. However, recent discoveries have found that three-dimensional (3D) cell culture models offer benefits that 2D cultures cannot. For example, in 2D cultures, cancer cells rely on adherence to a flat surface and thus all cells are exposed to a similar amount of nutrients and growth factors, but 3D cultures can more closely mimic the *in vivo* environment where cells in the center of a tumor would be hypoxic and have reduced proliferation.

One type of 3D cell culture model system utilizes the growth of cancer cell lines in low-attachment cell culture flasks and serum-free media, which produces spherical, free-floating cells, which are named tumorspheres or spheroids. This type of cell

culturing allows for the growth and expansion of a subpopulation of cells from the overall cell line, in which the cells show characteristics of cancer stem cells. The first description of cancer stem cells in free-floating culture came from the dissociation of brain tumors (Singh, et al., 2003) and in the subsequent years, a wide range of solid tumors and cancer cell lines have given rise to spheroids. This type of stem cell shares characteristics with typical stem cells such as self-renewal and pluripotent capacity (Reya, Morrison, Clarke, & Weissman, 2001). Although they have these features, cancer stem cells are a distinct population of cells that are essential for the development of a tumor and their relationship to the overall population of cells in culture is unknown.

<div align="center">Risk Factors of Urinary Carcinoma</div>

The lifestyle choices that we make have a large impact on our health. Some of these decisions leave us more susceptible to developing specific types of cancer. For urinary carcinoma, many risk factors increase a person's chances of developing this type of cancer. To illustrate this, research has found that men who smoke have a two-fold increase in developing bladder tumors, while women who smoke have a four-fold increase compared to those who never smoke (Reedman, Silverman, Hollenbeck, Schatzkin, & Abnet, 2011). On the contrary, there was found to be no association of alcohol and no strong association of coffee with urinary carcinoma (Pelucchi & La Vecchia, 2009).

Environmental risk factors also play a role in the development of urinary tumors. For those who reside in Egypt and other countries in the eastern hemisphere, *schistosoma haematobium* (*S. haematobium*), whose life cycle is in freshwater snails and humans, has been found to cause 27% of urinary carcinoma cases in Cairo, Egypt (Elsebai, 1977). The most notable environmental risk factor of urinary carcinoma is occupational exposures.

Over a century ago, it was first noted that dye workers in Germany were found to have incidence of bladder tumors (Johansson & Cohen, 1998). It was found that the causative agent was 2-Naphthylamine, a now recognized carcinogenic agent of bladder cancer (Humans, 2010). Since then, it has been estimated that urinary carcinoma from occupational exposures has resulted in up to 27% of the total number of cancers (Delclos & Lerner, 2008).

Heavy Metals

Of particular interest to our laboratory are the heavy metals arsenic and cadmium (Cd^{2+}), two of the four heavy metals that are known to be carcinogenic to humans (Ernst & Theriault, 1984). Since both of these heavy metals have been associated with an increased risk of many cancers, they have been designated by the International Agency for Research as a Group 1 human carcinogen (Cancer, Cadmium and Cadmium Compounds, 1993) (Cancer, Arsenic and Arsenic Compounds, 2002).

Exposure and Metabolism of Arsenic

Of the three biological groups of arsenic compounds, inorganic arsenic (iAs) is associated with acute and chronic effects through two common ways of exposure: inhalation from industrial sources or ingestion of contaminated drinking water. In addition, arsenic is present in soil with concentrations up to 40µg/g (Cancer, Monographs on the Evaluation of the Carcinogenic Risk of Chemicals to Man: Some Metals and Metallic Compounds, 1980), which contaminates crops. This has negative implications on rice, which is ten times more effective at absorbing arsenic compared to other grains (Schmidt, 2015). Given the strong evidence of adverse health effects that can be attributed to iAs

exposure, understanding the metabolism of this metalloid is a necessary part to elucidating its role in carcinogenesis.

iAs comes in two forms: arsenite (As^{3+}) and arsenate (As^{5+}), of which As^{3+} is the more common of the two. Once in the body, iAs can be metabolized by participation in oxidation-reduction reactions and methylation. This happens when As^{5+} is reduced to As^{3+} and this product can undergo oxidative methylation. The methylation of As^{3+} plays an important role in the metabolism of iAs as it is converted into mono-methylated (MMA) and di-methylated (DMA), which are secreted in urine. DMAs are the predominant metabolite secreted in the urine, accounting for 60-80% of iAs (Drobna, Styblo, & Thomas, 2009). Subsequent studies on methylated arsenals found these metabolites were strong cytotoxins and inhibitors of enzymes, even more so than As^{3+} (Thomas, Styblo, & Lin, 2001). Taken together, it should be known that the metabolism of iAs produces more reactive species that could play a role in the toxicity and carcinogenic of arsenic. An alternative model of the methylation of arsenic has been proposed. Instead of undergoing oxidative methylation, arsenic is bound to cellular thiols and this is the substrate for its methylation. The formation of the arsenic-thiol complexes, which could be cellular thiols or in glutathione (GSH), which undergo hydrolysis rather than oxidative methylation (Hayakawa, Toru, Kobayashi, Cui, & Hirano, 2005).

The Role of Arsenic and Carcinogenesis

The mechanisms of which arsenic causes the development of cancer in humans has not been fully elucidated. As previously illustrated, the metabolism of arsenic may induce the production of toxic free radicals, which can cause damage to lipids, proteins, and deoxyribonucleic acid (DNA). In addition, As^{3+} exposure to multiple mammalian cell lines induced the expression of mitogen-activated protein kinase (MAPK) pathways,

intermediate early genes (IEGs), and the activation of the transcription factor activator protein 1 (AP-1) (Beyersmann, 2002). The expression of these pathways and genes supports the hypothesis that cell proliferation occurs in response to arsenic, which may lead to neoplastic growth. Furthermore, other studies found that As^{3+} inhibited the activation of nuclear factor kappa-light-chain-enhancer of activated B cells (NF-κB) by the inhibition of I-κB kinase, which is required for phosphorylation and subsequent degradation of the I-κB inhibitor (Kapahi, et al., 2000). This in turn leads to a down regulation of NF-κB induced genes and stimulation of cell proliferation.

Arsenic and its Implications in Urinary Carcinoma

There is mounting evidence showing arsenic is carcinogenic to humans, specifically causing cancers of the bladder, lung, kidney, and skin. With millions of people around the globe consuming drinking water contaminated with arsenic, this is a significant cause of urinary carcinoma. The current United States drinking water standard for arsenic is at or below a concentration of 10 parts per billion, but it is estimated that over 300,000 people drink water with arsenic levels above the set standard level (Corporation, 1987).

The most extensive epidemiological studies on the effects of iAs and urinary carcinoma were conducted on a population of individuals that inhabited the southwest coast of Taiwan. With deep artesian wells contaminated with arsenic, endemic rates of blackfoot disease, pigmented, and hyperkeratotic skin lesions were detected. This prompted researchers to study rates of cancer in the area and found the mortality risk ratios for bladder cancer was 28.7 for men and 65.4 for women at the highest level of arsenic exposure, where a risk ratio of greater than one is interpreted as the outcome is increased by the exposure (Smith, et al., 1992). Despite this promising looking evidence, it has been suggested that

29

the arsenic in the water was not the sole cause of cancer and averages from large groups instead of individual exposure data was used to draw conclusions, which may render this study showing false results.

More recent studies have considered the criticisms of the study in Taiwan and provided evidence that ingested arsenic does indeed lead to the development of urinary carcinoma. Two large studies took place in South America, the first being in a province of Argentina called Cordoba. The study found the average level of arsenic in their drinking water to be 178µg/L, which caused their mortality rates of urinary carcinoma to be double the national average (Hopenhayn-Rich, et al., 1996). The second study which took place in Northern Chile found mortality of urinary carcinoma was six to eight fold higher in a population exposed to river water with arsenic levels of approximately 600µg/L (Smith, Goycolea, Haque, & Biggs, 1998).

Contrary to the aforementioned studies, a population-based case-control study in southeastern Michigan exposure individuals to between 10 and 100µg/L of arsenic found no increase in urinary carcinoma risk. This study included 411 cases of cancer and found when comparing those who were exposed to >10µg/L to those who were exposed to <1µg/L, there was no evidence an association between arsenic exposure at low-level concentrations and urinary cancer (Meliker, et al., 2010).
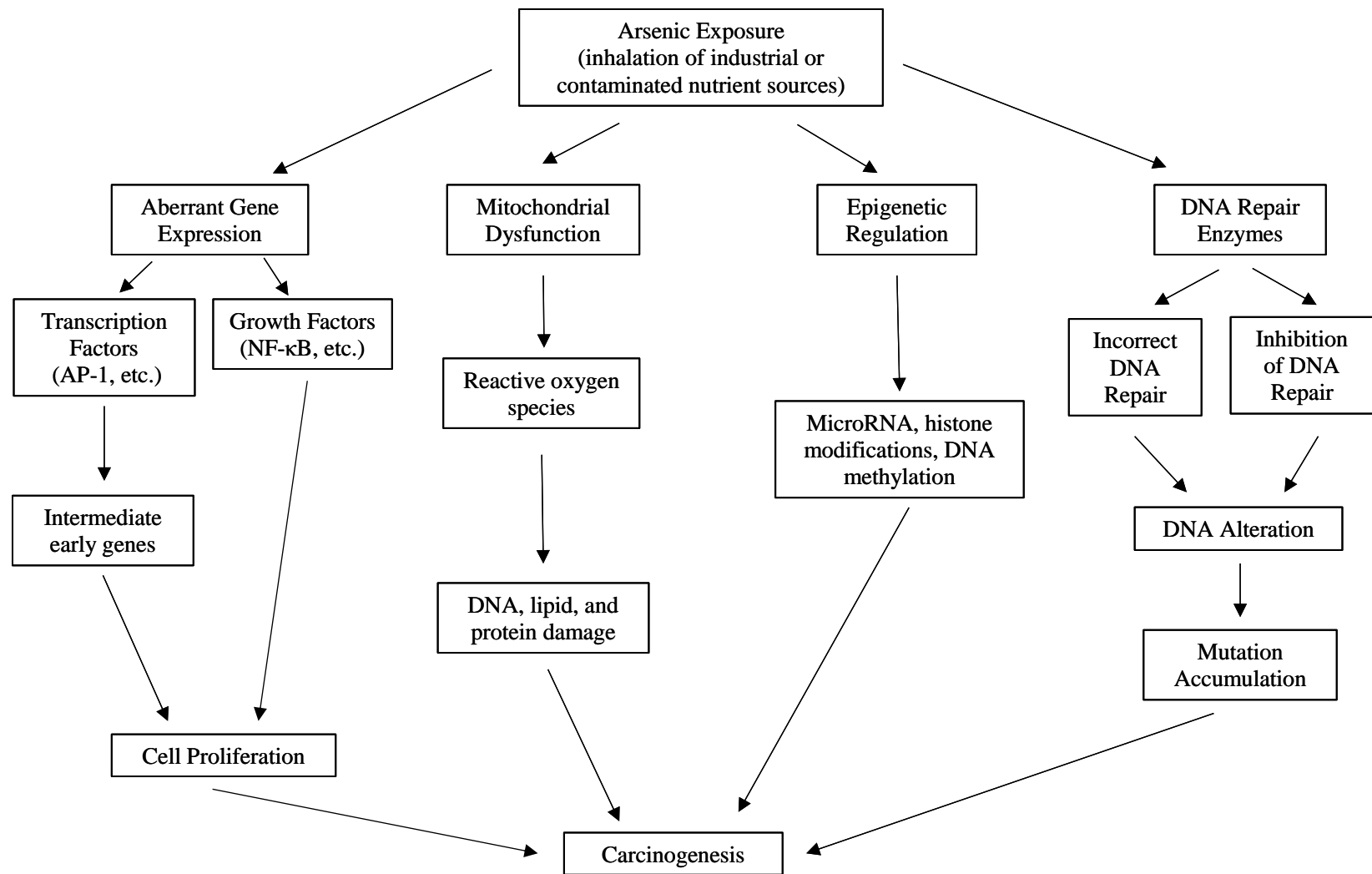
Figure 2. Proposed mechanisms of arsenic toxicity and carcinogenesis (Adapted from Kitchin & Wallace, 2007 and Li & Chen, 2016).

Exposure and Metabolism of Cadmium

Humans are exposed to Cd^{2+} via a few sources such as inhalation of industrial pollution, contamination of top soil, which is absorbed into growing plants, and cigarette smoking. The average human intakes between 1-3µg/day of cadmium and this amount is doubled in smokers who consume a pack a day (Registry, 2012). The half-life of Cd^{2+} in humans is estimated to be more than 20 years (Satarug, et al., 2005), which allo ws it to be efficiently trapped in the body and cause toxicity.

Once Cd^{2+} is in the body, it is transported via receptors in different types of cells where it undergoes metabolism by binding to members of the metallothionein (MT) family. MTs are proteins that are rich in cysteine and the major zinc-binding protein (Klaassen, Liu, & Choudhuri, 1999). By binding to MTs, Cd^{2+} is unable to participate in other reactions and is subject to detoxification. A second intracellular Cd^{2+} scavenger is glutathione (GSH), an intracellular thiol. The Cd^{2+}-GSH complex leads to the detoxification of Cd^{2+} (Mah & Jalilehvand, 2010).

The Role of Cadmium and Carcinogenesis

Exposure to Cd^{2+} has many implications in the body, such as induction of IEGs and other detoxifying genes, increased production of reactive oxygen species (ROS), and interactions with DNA damage repair systems. Similar to arsenic, Cd^{2+} induced the overexpression of IEGs, which play a role in the stimulation of cell proliferation. This implicates Cd^{2+} toxicity in promoting multi-stage carcinogenesis (Cohen, 1998). Under physiological conditions, Cd^{2+} does not participate in reduction-oxidation reactions, but oxidative stress is implicated to play a role in cadmium-induced carcinogenesis. A study found increased levels of ROS both *in vitro* and *in vivo*, which is mediated by Cd^{2+} exerting an inhibitory effect on antioxidant enzymes (Lui, Qu, & Kadiiska, 2009). These reactive

species could lead to chromosomal aberrations, gene mutations, and DNA damage (Joseph, 2009).

There is evidence that Cd^{2+} disrupts three types of DNA repairs systems: base excision repair (BER), nucleotide excision repair (NER), and mismatch repair (MMR). Under normal conditions, BER corrects small lesions in the DNA by glycosylases that identify damaged bases, recognition of apyrimidinic/apurinic sites, cleavage of these sites, and synthesis the correct bases by DNA polymerase (Memisoglu & Samson, 2000). Cd^{2+} affects the initial step of BER, the recognition and removal of damaged bases by inactivated proteins involved in these steps . (Giaginis, Gatzidou, & Theocharis, 2006). NER functions to correct larger, damaged pieces of DNA by unwinding the DNA, generating incisions and excising the DNA, and repair by DNA polymerase and ligase (Costa, Chigança, da Silva Galhardo, Carvalho, & Mench, 2003). It has been found that Cd^{2+} by substituting itself for zinc and by binding to negatively charged molecules and changing the confirmation and disturbing DNA-protein interactions that are essential for the repair process (Giaginis, Gatzidou, & Theocharis, 2006). MMR systems repair DNA mismatches that occur from replication and recombination by recognizing and excising the incorrect DNA and synthesizing the correct DNA using the parental strand as a template (Hsieh, 2001). Like BER, Cd^{2+} affects the initial step of base repair by interfering with ATP binding and the hydrolysis enzymes of MMR enzymes, which reduce the ability of their binding affinity and their function to discriminate between correct and mismatched bases (Giaginis, Gatzidou, & Theocharis, 2006).

Cadmium and its Implications in Urinary Carcinoma

Epidemiological studies focusing on the association between Cd^{2+} and urinary carcinoma have found contradicting studies which show both no evidence and significant evidence of this association. A study that looked at the concentrations of Cd^{2+} in red blood cells and plasma found no significant difference in those with urological malignancies compared to those with benign diseases (Feustel & Wennrich, 1986). A more recently conducted case-controlled study in Montreal, Canada found a weak association between occupational exposure to Cd^{2+} and an increased risk of urinary carcinoma (Siemiatycki, Dewar, Nadon, & Gérin, 1994). Furthermore, two case-controlled studies in Tunisia and Belgium found increased levels of Cd^{2+} blood concentrations were associated with an increased risk of bladder cancer (Feki-Tounsi, et al., 2013) (Kellen, Zeegers, Hond, & Buntinx, 2007). Taken together, albiet the study by Feustel & Wennrich found no evidence of urinary carcinoma and Cd^{2+} exposure, others studies have demonstrated an association between increased risk of urinary carcinoma and Cd^{2+} exposure.
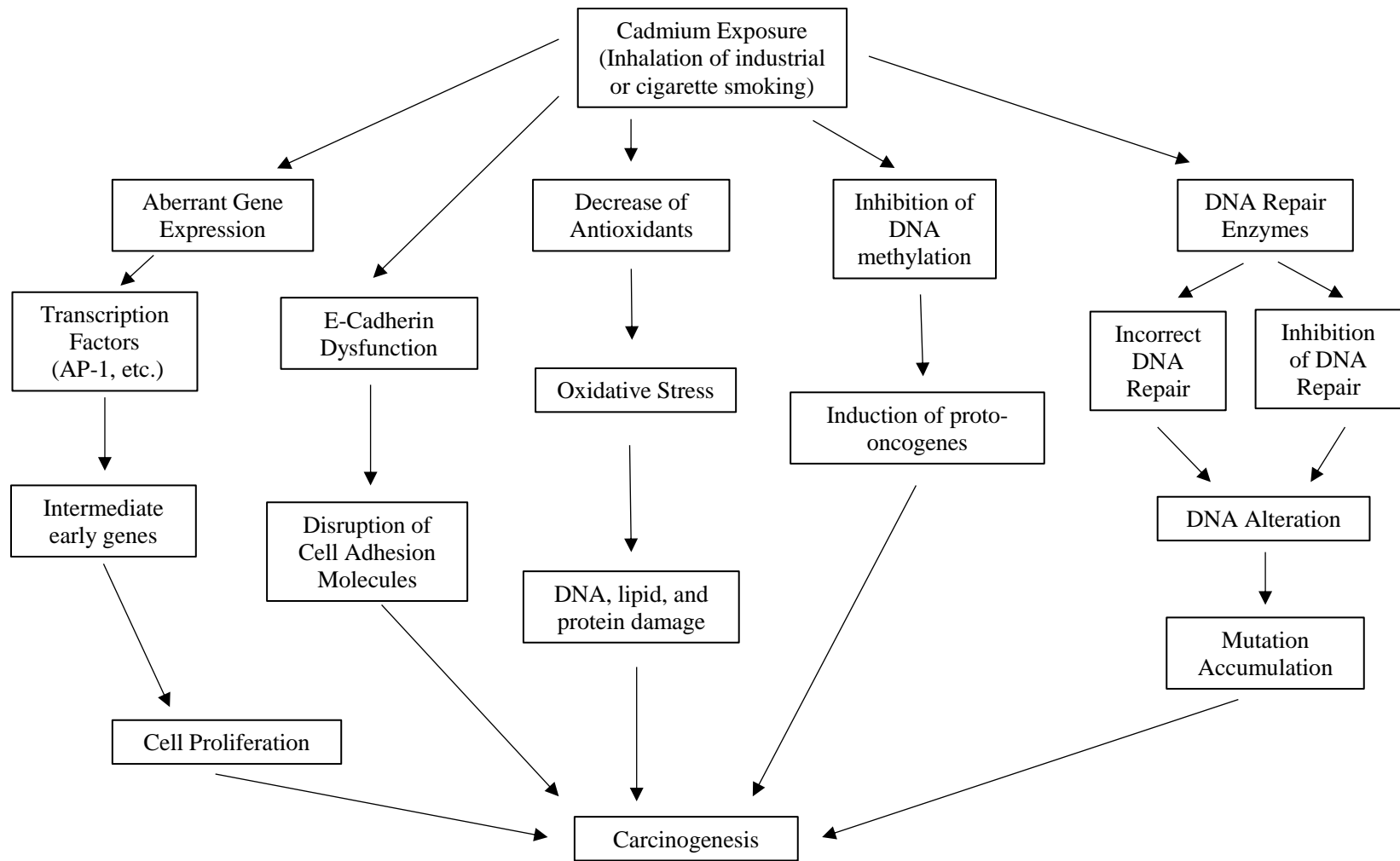
Figure 3. Proposed mechanisms of cadmium toxicity and carcinogenesis (Adapted from Waisberg, Joseph, Hale, & Betersmann, 2003).

Experimental Models

UROtsa

The UROtsa model was initially cultured from ureter cells of a 12-year old female and subsequently immortalized via the SV40 large T antigen. Although immortalized, the cells did not display properties of neoplastic cells such as growth on soft agar and subsequent tumor development in athymic mice (Petzoldt, Leigh, Duffy, Sexton, & Masters, 1995). These cells form an undifferentiated monolayer in culture, but under serum-free conditions have shown to undergo partial differentiation and resemble structures of the intermediate layer of the bladder; specifically there were areas of multicellular organoid structures that contained abundant intermediate filaments resembling a differentiated intermediate layer of the bladder urothelium. (Rossi, et al., 2001). In addition, the UROtsa cell line was transformed via exposure to 1µM sodium arsenite ($NaAsO_2$) or 1µM cadmium chloride ($CdCl_2$), which led to the creation of six As^{3+} and seven Cd^{2+} independently transformed cell lines. In contrast to the parental cell line, both of the transformed lines produced growth of colonies on soft agar and tumors in athymic mice (Sens, et al., 2004). Taken together, this model allows for comparison between the cultured cell lines and their corresponding heterotransplant tumors.

Goals of the Present Study

This study was performed in two parts in order to further our understanding of muscle-invasive urinary carcinoma and cancer stem cells isolated from the cancer cell lines. Muscle-invasive bladder cancer has been shown to have 5-year survival rates of only 15% of patients who have been diagnosed with stage T4 urinary carcinoma (Goebell & Knowles, 2010). In the first part of the study, we first sought to determine if heterotransplant tumors generated from the transformed UROtsa cell culture model are

enriched in markers of the basal subtype of muscle-invasive urinary carcinoma. Secondly, was to determine if the UROtsa cell lines transformed by As^{3+} and Cd^{2+} also reflect the basal subtype of muscle-invasive urinary carcinoma and if this subtype signature is enriched in the putative cancer stem cells isolated from the corresponding transformed cell lines. Lastly, we wish to determine if the parental UROtsa cell line contains a population of putative cancer stem cells, which have a gene signature of the basal subtype of muscle-invasive bladder cancer. To address the above questions, we determined the expression level of 9 basal and 16 luminal markers in the heterotransplant tumors, cell lines, and spheroids, and performed western blotting of the cell lines and immunohistochemical staining of tumors. By understanding which subtype of muscle-invasive urinary carcinoma our model system fits, we can further characterize our UROtsa model and can study a toxicity-based carcinogenic model of muscle-invasive bladder cancer.

The second part of this study was to determine the stability of the putative cancer stem cell gene signature of the parental UROtsa and As^{3+} and Cd^{2+} transformed isolated cancer stem cells when cultured under conditions identical to the parent culture and serum-free culture conditions, which are used to isolate the cancer stem cells. Our laboratory has previously cultured the parental UROtsa cells under serum-free culture conditions and found the cells, once confluent, developed multicellular organoid structures containing intermediate filaments and cells located apically in the structures appeared to be more differentiated (Rossi, et al., 2001). To do this, triplicate samples of the putative cancer initiating cells were grown in regular culture flasks in serum-containing media or in serum-free media. Total RNA samples were isolated when the

37

spheroids reach confluency (P1), and passages 4 and 8 (P4 and P8). The ability to

investigate the differences found in the gene expression between the original cell line and

its spheroid and the stability of the gene signature will allow us to better understand the

interactions of these two distinct cell populations in culture and how putative cancer stem

cells react with their culture environment in chronic response studies.

CHAPTER II

METHODS

Cell Culture

URObsa cells were initially cultured and developed in order to provide an *in vitro* model of normal urothelium (Petzoldt, Leigh, Duffy, Sexton, & Masters, 1995) and further characterized in this laboratory (Rossi, et al., 2001). The cells were cultured in serum-containing media, which was composed of Dulbecco's modified Eagle's medium (DMEM) (Sigma-Aldrich, St. Louis, MO; D5523) supplemented with 5% vol/vol fetal bovine serum (FBS) (Gibco/ThermoFisher Scientific, Grand Island, NY; 16000-044) and serum-free media, which was composed of of a 1:1 mixture of DMEM and Ham's F-12 (Sigma-Aldrich, St. Louis, MO; N6760) supplemented with insulin (5g/mL), transferrin (5g/mL), hydrocortisone (36ng/mL), epidermal growth factor (10ng/mL), selenium (5ng/mL), and triiodothyronine (4pg/mL). Both types of media cultures were incubated at 37°C in 5% CO_2:95% air atmosphere. Upon reaching confluency, cells were subcultured at a 1:4 ratio using trypsin-EDTA (0.05%, 0.02%) and fed fresh growth medium every three days.

In the interest of gaining valuable knowledge of the toxic effect of As^{3+} and Cd^{2+} on urothelial cells, a model of metal-induced urothelial carcinoma was created using the URObsa bladder cell line. To do this, URObsa cells were transformed by culturing the cells with media which contained either 1μM $NaAsO_2$ (Sigma-Aldrich, St. Louis, MO;

S7400) or 1µM CdCl$_2$ (Sigma-Aldrich, St. Louis, MO; C1016). The cells were continued to be exposed to these metals and were tested for their ability to form colonies on soft agar every 5 passages (Sens, et al., 2004).

For the formation of the spheroids, cells from the parental UROtsa, six As^{3+} and seven Cd^{2+}-transformed cell lines were seeded in T-25cm^2 Ultra-low attachment flasks (Corning Inc., Corning NY; CLS3815) at a density of 1 x 10^5 cells. The serum-free growth medium for these cells is mentioned above. The cells were allowed to form spheres for eight days before harvesting by centrifugation for RNA isolation.

Animals

The mouse heterotransplants were produced as previously described (Sens, et al., 2004). Briefly, the As^{3+} and Cd^{2+}-transformed cell lines were injected at a dose of 1 x 10^6 cells in the dorsal thoracic midline of athymic nude (NCr-*nu*/*nu*) mice. Mice were sacrificed ten weeks post-implantation or when clinical conditions dictated by CO$_2$ inhalation and euthanasia and conformed to American Veterinary Medical Association Guideline on Euthanasia. This study was approved under protocol IACUC #1117-2C by the University of North Dakota Care Committee and adhered to all recommendations in the Guide for the Care and Use of Laboratory Animals of the NIH.

RNA Isolation and Real-Time RT-PCR

After cells were harvested by cell scraping and pelleted via centrifugation, total RNA was isolated using TRI Reagent (Molecular Research Center, Inc., Cincinnati, OH; TR 118) according to manufacturer's instructions. Total RNA of 0.1µg was purified from the cell lines, urospheres, and tumor heterotransplants and subjected to cDNA synthesis using the iScript cDNA Synthesis Kit (Bio-Rad Laboratories, Hercules, CA;

1708891BUN) in a total volume of 20µL. Real-time RT-PCR was performed using the

SsoAdvanced Universal SYBR Green Supermix (Bio-Rad Laboratories, Hercules, CA;

1725274) with 2µL of cDNA and 0.2µM of primers (Bio-Rad Laboratories, Hercules,

CA and Qiagen, Valencia, CA) in a total volume of 20µL in a CFX96 Touch Real-Time

PCR Detection System (Bio-Rad Laboratories, Hercules, CA; 1855195). Cycling

parameters are as follows: denaturation at 95°C for 15 seconds, annealing at 60°C for 30

seconds, and an extension at 72°C for 30 seconds and amplification was monitored via

SYBR green fluorescence.

Immunohistochemistry

Tumor tissue from mouse tumor transplants was fixed in 10% neutral-buffered

formalin for 16-18 h. The fixed tissue samples were transferred to 70% ethanol and

dehydrated in 100% ethanol. The dehydrated tissue samples were cleared in xylene,

infiltrated, and embedded in paraffin. Serial sections were cut at 3-5µm for use in

immunohistochemical protocols. Prior to immunostaining, sections were immersed in

preheated Target Retrieval Solution (Dako, Carpinteria, CA) and heated in a steamer for

20 min. The sections were allowed to cool to room temperature and immersed into TBS-

T for 5 min. The primary antibodies were localized using Dako peroxidase conjugated

EnVision plus for rabbit primary antibodies or a Dako peroxidase conjugated EnVision

plus dual link antibody for mouse primary antibodies at room temperature for 30 min.

Liquid diaminobenzidine (Dako) was used for visualization. Counter staining was

performed for 8 min. at room temperature using Ready-to-use Hematoxylin (Dako).

Slides were rinsed in distilled water, dehydrated in graded ethanol, cleared in xylene, and

cover-slipped. Two pathologists judged the presence and degree of immune-reactivity in

41

the specimens. The scale used was 0 to +3 with 0 indicating no staining, +1 staining of mild intensity, +2 staining of moderate intensity, and +3 staining of strong intensity.

Table 1. Immunohistochemical Analysis Antibodies

Antigen	Source	Cat. No.	Dilution/Concentration
Keratin 1	Invitrogen	PA5-26699	1:100
Keratin 5	Invitrogen	PA5-29670	1:400
Keratin 6	Santa Cruz	sc-514520	1:500
Keratin 7	Dako (Agilent)	M7018	1:50
Keratin 14	Invitrogen	PA5-16722	1:400
Keratin 16	Abcam	ab8741	1:40
Keratin 17	Dako (Agilent)	M7046	1:20
Keratin 19	Abcam	ab15463	1:100
Keratin 20	Invitrogen	PA5-22125	1:100
CD44	R&D Systems	MAB7045	10μg/ml
P-cadherin	Santa Cruz	sc-7893	1:200
TP63	Abnova	MAB10290	1:100
CD24	Invitrogen	MA5-11833	1:10

Statistical Analysis

Statistical analysis consisted of Fisher's LSD testing performed by Graphpad PRISM 7.02. All experiments were done in triplicates and the data is plotted as the mean ± SEM or ± SD of triplicate determination.

CHAPTER III

RESULTS

Basal and luminal marker gene expression in As^{3+} and Cd^{2+}-transformed UROtsa

cell derived tumor transplants

The gene signature patterns that identify normal and malignant breast cancer

tissue has led researchers to study if these unique patterns exist in other tissue types. Choi

and coworkers identified 25 marker genes (Table 2) that define the basal and luminal

subtype of muscle-invasive bladder cancer (MIBC) (Choi, et al., 2014). Using these

genes, the expression of tumor transplants generated from the As^{3+} and Cd^{2+}-transformed

UROtsa cells was determined to see if they associated with the basal or luminal subtypes

of MIBC. To do this, total RNA was isolated from the tumors of the six As^{3+} and seven

Cd^{2+}-transformed cell lines and subjected to real-time RT-PCR analysis of the 25 marker

genes. In addition, the tumors were analyzed for and then normalized to five

housekeeping genes, ACTB (β-actin), B2M (β-2-microglobulin), HPRT1 (hypoxanthine

phosphoribosyltransferase 1), RPLP0 (60S acidic ribosomal protein P0), and UBC

(ubiquitin C). This was done so that direct comparison of the mRNA from the UROtsa

tumors and the 73 primary MIBCs selected by Choi could be compared (Choi, et al.,

2014)

Table 2. Real-Time RT-PCR Analysis Primers

Gene	Molecular Subtype	Catalog No./Unique Assay ID No.	Company
CD24	Luminal	QT00216811	Qiagen
CYP2J2	Luminal	qHsaCID0016825	Bio-Rad
ERBB2	Luminal	qHsaCID0012766	Bio-Rad
ERBB3	Luminal	qHsaCID0018397	Bio-Rad
FABP4	Luminal	qHsaCID0036778	Bio-Rad
FGFR3	Luminal	qHsaCED0042267	Bio-Rad
FOXA1	Luminal	qHsaCED0002547	Bio-Rad
GATA3	Luminal	qHsaCID0017793	Bio-Rad
GPX2	Luminal	qHsaCID0014084	Bio-Rad
KRT7	Luminal	qHsaCED0038533	Bio-Rad
KRT8	Luminal	qHsaCED0038745	Bio-Rad
KRT18	Luminal	qHsaCED0035037	Bio-Rad
KRT19	Luminal	qHsaCED0046788	Bio-Rad
KRT20	Luminal	qHsaCID0007981	Bio-Rad
PPARG	Luminal	qHsaCED0044425	Bio-Rad
XBP1	Luminal	qHsaCID0010491	Bio-Rad
CDH3	Basal	qHsaCID0015341	Bio-Rad
CD44	Basal	qHsaCID0013679	Bio-Rad
KRT1	Basal	qHsaCID0011275	Bio-Rad
KRT5	Basal	qHsaCED0005398	Bio-Rad
KRT6A	Basal	qHsaCED0036985	Bio-Rad
KRT6B	Basal	qHsaCED0003069	Bio-Rad
KRT6C	Basal	qHsaCED0046712	Bio-Rad
KRT14	Basal	qHsaCED0047868	Bio-Rad
KRT16	Basal	qHsaCED0047866	Bio-Rad
KRT17	-	qHsaCID0023841	Bio-Rad
TP63	-	qHsaCIP0039056	Bio-Rad

Following normalization, a Principal Component Analysis (PCA) was performed on the integrated data. The first principal component explained 52.63% of the total variation and the second principal component explained a further 17.43%, which totals to 70.06% of the total variation explained in these two principal components. As visualized in the PCA plot (Figure 4A), the transplanted tumors generated from the As^{3+} and Cd^{2+}-transformed UROtsa cell lines had similar expression patterns, except for one sample (As#5), in the first principal component, PC1. In addition, total RNA isolated from the

parental UROtsa cells was subjected to PCA and it was found to be distinct from the

MIBC and As^{3+} and Cd^{2+}-transformed tumor samples.

Unsupervised hierarchical clustering was employed to determine the tumor

subtypes of the As^{3+} and Cd^{2+} transformed tumors. Analysis of the data found that the

samples clustered into three distinct groups located at the top, middle, and bottom of the

dendrogram (Figure 4B). The group at the top showed high expression of the luminal

marker genes and low expression of the basal marker genes. Conversely, the group at the

bottom showed low expression of the luminal marker genes and high expression of the

basal marker genes. The group located in the middle showed neither high nor low

expression of the basal and luminal marker genes. All of the tumor transplants generated

by the As^{3+} and Cd^{2+} transformed cell lines clustered with the basal subtype of MIBC

located at the bottom of the dendrogram. The cluster made by the UROtsa samples can be

further divided into two subtypes: one that consists of six tumors from the Cd^{2+}

transformed cells (Cd #2, Cd #4, Cd #5, Cd #6, and Cd #7) and three isolates of the As^{3+}

(As #2, As #3, and As #5) and the second which consist of one Cd^{2+} isolate (Cd #1), three

As^{3+} isolates (As #1, As #4, and As #6). The parental UROtsa cell line sample has a

distinct expression pattern not associated with any of the three subtypes.
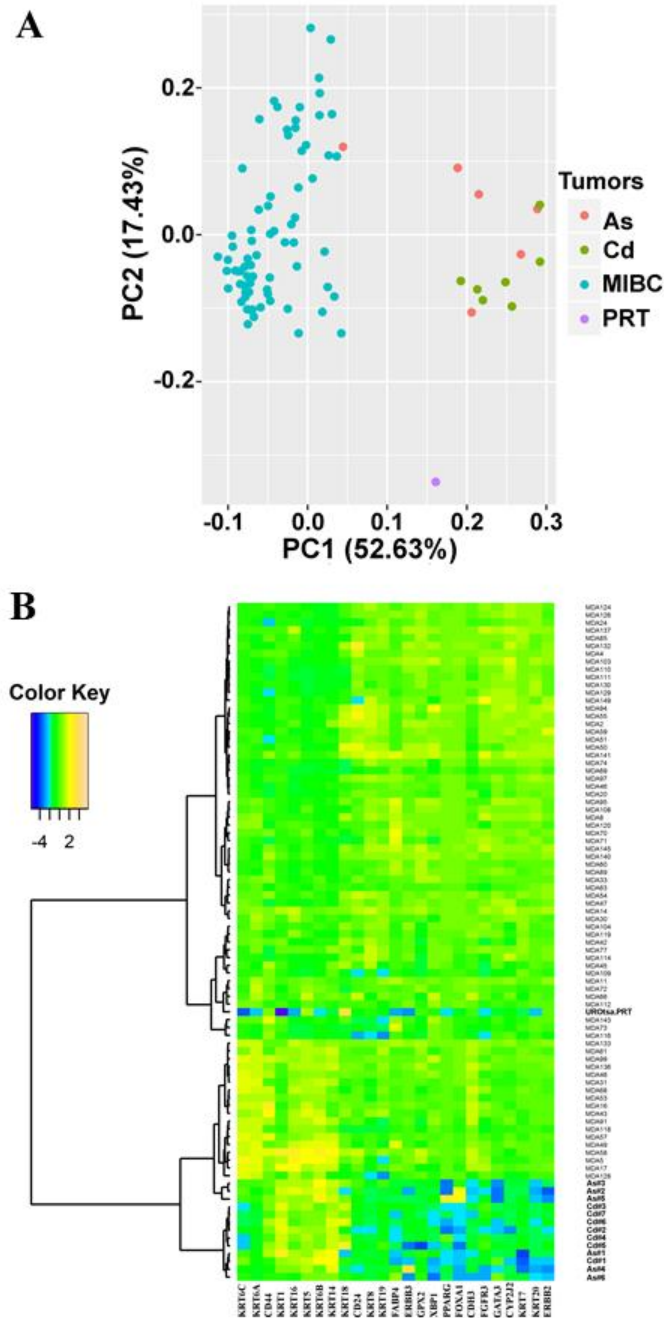
Figure 4. Gene expression pattern analysis in the As^{3+} and Cd^{2+} tumor transplants.
(A). Principal component analysis (PCA) plot of the As^{3+} and Cd^{2+} tumor transplants,
MIBCs, and parental UROtsa cell line. The principal components, PC1 and PC2, were
calculated form the 25 MIBC marker genes. (B). Heat map and dendrogram of the 25
MIBC marker genes. Each column represents one of the 25 marker genes and each row
represents a tumor sample. The dendrogram was generated using hierarchical clustering
based on Pearson's dissimilarity and Ward's linkage.

46

The expression of 25 MIBC marker genes was determined for the tumor heterotransplants generated from the six independent isolates of the As^{3+} and seven independent isolates of the Cd^{2+}-transformed UROtsa cells (Figure 5A and 5B). Analysis of the gene expression profiles demonstrated a clear trend for higher expression of genes associated with the basal subtype of MIBC. A few exceptions were noted; the first was that all the tumors displayed low expression P-cadherin (CDH3), a marker of basal MIBC. The second was the elevated expression of KRT19 compared to the other luminal marker genes.
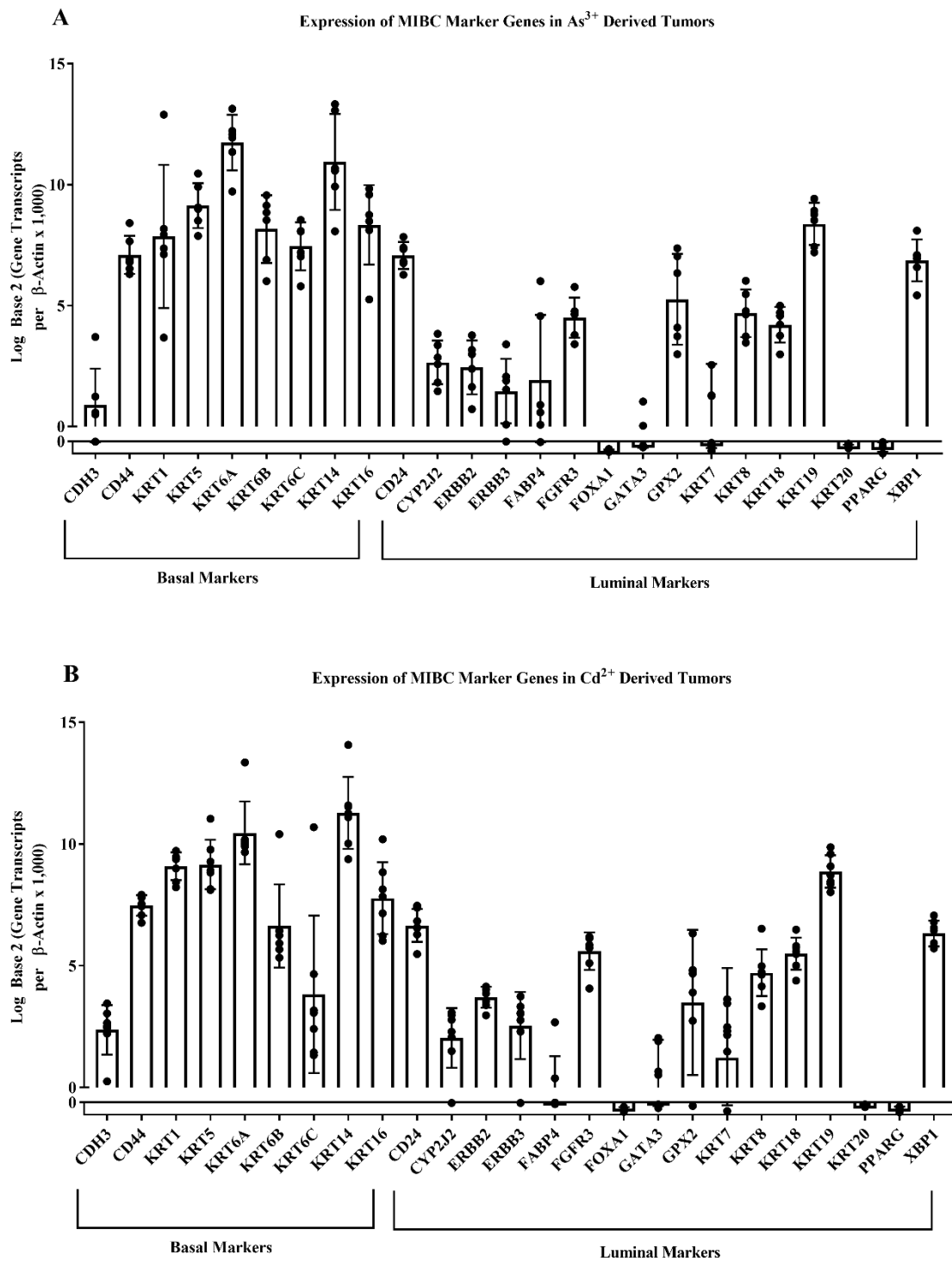
Figure 5. Gene expression analysis of basal and luminal marker genes in the heterotransplant tumors produced by the As^{3+} and Cd^{2+}-transformed UROtsa cells. Real-time RT-PCR analysis of basal and luminal marker genes in the As^{3+} (A) and Cd^{2+} (B) heterotransplants. The analysis was done in triplicates and plotted as ± SD on a log base 2 scale per transcript of β-actin times 1,000.

48

Immunohistochemical expression and localization in As³⁺ and Cd²⁺-transformed

UROtsa cell derived tumor transplants

Immunohistochemical analysis was executed on tumors generated from the As³⁺

and Cd²⁺-transformed cells lines in order to determine the localization and expression

level of the basal and luminal marker genes. Except for CHD3, there was positive

staining for all of the basal markers in the tumors. A representative staining of each of the

basal markers is shown for the tumor generated from the As³⁺ (As #3) (Figure 6) and

Cd²⁺ (Cd #3)-transformed cell line (Figure 7). An independent assessment by two

pathologists found the percent of individual tumors with positive staining for each basal

marker in conjunction with the level of expression judged on a scale from 0 to +3 (Table

3) and the percent of tumor cells stained for each of the basal markers. The level of

expression for each of the basal markers was found to be strong for the tumors, with

expression intensities between +2 and +3. KRT5 was found to the basal marker with the

highest percentage of stained tumor cells, with percentages between 70 and 90%. The

lowest number of stained tumor cells was found when staining for KRT16, with

percentages between 5 and 50%. The other basal markers were found to be intermediate

between these two markers and generally followed the pattern of KRT5 > KRT1 >

KRT14 ≥ CD44 > KRT6 > KRT16. No correlation was found between the mRNA levels

of the individual tumor isolates and staining intensities for the basal marker genes.

Table 3. Immunostaining of basal protein markers in As^{3+} and Cd^{2+} tumor transplants.

Group	KRT1		KRT5		KRT6		KRT14		KRT16		CD44	
	INT	%	INT	%	INT	%	INT	%	INT	%	INT	%
As #1	3+	60	3+	90	3+	20	3+	90	3+	10	3+	70
As #2	3+	50	3+	80	3+	60	3+	80	3+	40	3+	60
As #3	3+	50	3+	90	3+	60	3+	80	3+	20	3+	30
As #4	3+	40	3+	90	3+	60	3+	90	3+	50	3+	70
As #5	3+	40	3+	80	2+	60	3+	30	3+	20	3+	30
As #6	3+	70	3+	90	3+	40	3+	90	3+	40	3+	50
Cd #1	3+	50	3+	90	3+	60	3+	90	3+	40	3+	40
Cd #2	3+	50	3+	70	2+	20	3+	60	1+	<5	3+	70
Cd #3	3+	70	3+	90	3+	40	3+	30	2+	10	2-3+	40
Cd #4	3+	80	3+	90	3+	40	3+	50	2+	20	2-3+	50
Cd #5	3+	80	3+	90	3+	40	3+	60	2+	20	2-3+	30
Cd #6	3+	70	3+	90	2+	40	3+	60	2+	10	2-3+	50
Cd #7	3+	80	3+	90	3+	20	3+	50	2+	10	2-3+	50

INT: Intensity of staining
% : % of cells staining for a marker
3+ : Strong staining
2+ : Moderate staining
2-3+ : Moderate to strong staining
1+ : Weak staining
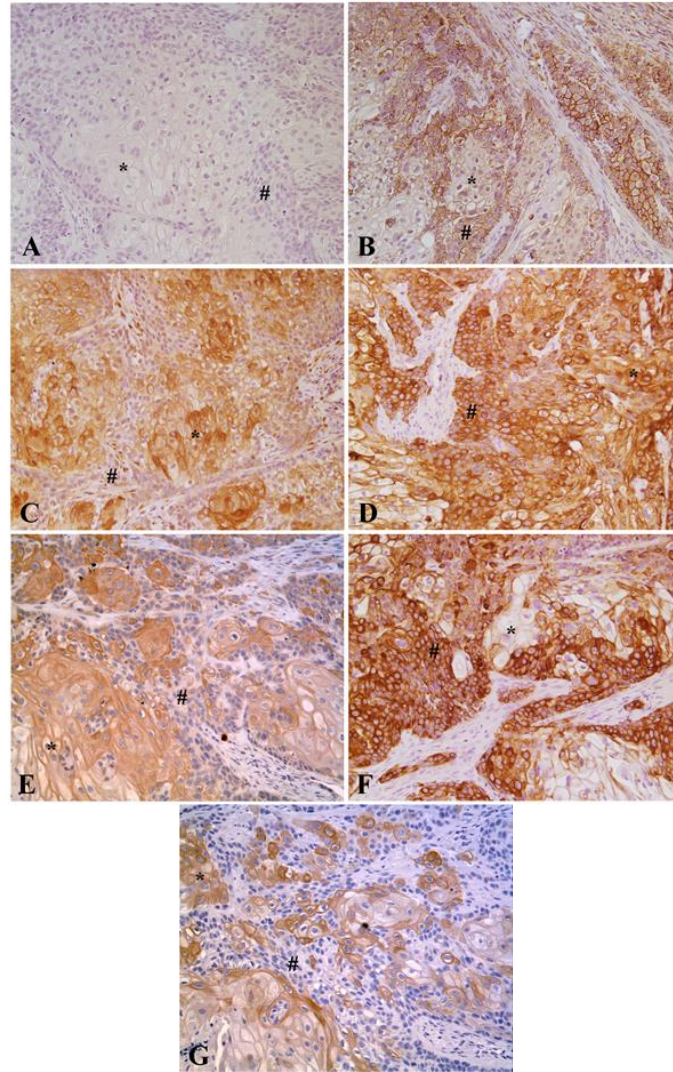
Figure 6. Immunohistochemical staining for basal gene markers in heterotransplant tumors generated from the As^{3+} transformed cell line (As #3). (A) CDH3. There is no staining in the well-differentiated or less differentiated areas of the tumor transplants. (B). CD44. There is no to weak staining in the center of the tumor nests, whereas the less differentiated peripheral cell membranes stain strongly for CD44. (C). KRT1. There is strong staining in the well-differentiated areas of the tumor, whereas the less differentiated cells show weak staining. (D). KRT5. There is strong staining in both the well- and less differentiated of the tumor. (E). KRT6. There is strong staining in the well-differentiated areas of the tumor, while the less differentiated areas show no to weak staining. (F). KRT14. The well-differentiated cells in the center of the tumor nests show no to weak staining and the less differentiated peripheral cells are strongly positive for KRT14. (G). KRT16. There is strong staining for KRT16 in the well-differentiated cells, whereas the less differentiated cells show no staining. * Indicates well-differentiated areas of the tumor. # indicates less differentiated areas of the tumor. The blue/purple color indicates the nuclei which are counterstained with hematoxylin and the brown color is indicative of the presence of the protein. Images are at a magnification of 200X.

Figure 7. Immunohistochemical staining for basal gene markers in heterotransplnat tumors generated from the Cd^{2+} transformed cell line (Cd #3). (A) CDH3. There is no staining in the well-differentiated or less differentiated areas of the tumor transplants. (B). CD44. There is no to weak staining in the center of the tumor nests, whereas the less differentiated peripheral cells stain strongly for CD44. (C). KRT1. There is strong staining in the well-differentiated, areas of the tumor, whereas the less differentiated cells show weak staining. (D). KRT5. There is strong staining in both the well-and less differentiated of the tumor. (E). KRT6. There is strong staining in the well-differentiated areas of the tumor, while the less differentiated areas show no to weak staining. (F). KRT14. The well-differentiated cells in the center of the tumor nests show no to weak staining and the less differentiated peripheral cells are strongly positive for KRT14. (G). KRT16. There is strong staining for KRT16 in the well-differentiated cells, whereas the less differentiated cells show no staining. * Indicates well-differentiated areas of the tumor. # indicates less differentiated areas of the tumor. The blue/purple color indicates the nuclei which are counterstained with hematoxylin and the brown color is indicative of the presence of the protein. Images are at a magnification of 200X.

The immunohistochemical analysis of the As^{3+} and Cd^{2+}-transformed UROtsa cell generated tumors identified distinct nests of cells are clusters of well-differentiated carcinoma cells, which are surrounded by stroma. The nests consisted of centers of well-differentiated cells with intracellular bridges and keratinization and less differentiated basal-like cells at the periphery. The staining intensity of the basal markers was distinct between these two areas for the tumors (Figures 6 and 7 and Table 3). It can be seen that the basal marker CD44 showed moderate to strong staining in the less differentiated, peripheral cells, whereas the well-differentiated cells at the center showed weak staining. In contrast, KRT1, KRT6, and KRT16 showed strong staining in the well-differentiated cells compared to the weakly stained less differentiated periphery cells.

Table 4. Localization of basal protein markers in different histological areas of the As^{3+} and Cd^{2+} tumor transplants.

Group	Well-differentiated cells in the center of tumor nests						Peripheral less differentiated cells					
	KRT1	KRT5	KRT6	KRT14	KRT16	CD44	KRT1	KRT5	KRT6	KRT14	KRT16	CD44
As #1	3+	3+	3+	3+	3+	0-1+	+1	3+	0-1+	3+	-	3+
As #2	3+	3+	3+	3+	3+	0-1+	+1	3+	0-1+	3+	-	3+
As #3	3+	3+	3+	0-1+	3+	0-1+	+1	3+	0-1+	3+	-	3+
As #4	3+	3+	3+	3+	3+	0-1+	+1	3+	0-1+	3+	-	3+
As #5	3+	3+	2+	0-1+	3+	0-1+	+1	3+	0-1+	3+	-	3+
As #6	3+	3+	3+	3+	3+	0-1+	+1	3+	0-1+	3+	-	3+
Cd #1	3+	3+	3+	3+	3+	0-1+	+1	3+	0-1+	3+	-	3+
Cd #2	3+	3+	2+	0-1+	1+	0-1+	+1	3+	0-1+	3+	-	3+
Cd #3	3+	3+	3+	0-1+	2+	0-1+	+1	3+	0-1+	3+	-	2-3+
Cd #4	3+	3+	3+	0-1+	2+	0-1+	+1	3+	0-1+	3+	-	2-3+
Cd #5	3+	3+	3+	0-1+	2+	0-1+	+1	3+	0-1+	3+	-	2-3+
Cd #6	3+	3+	2+	0-1+	2+	0-1+	+1	3+	0-1+	3+	-	2-3+
Cd #7	3+	3+	3+	0-1+	2+	0-1+	+1	3+	0-1+	3+	-	2-3+

3+ : Strong staining
2+ : Moderate staining
2-3+ : Moderate to strong staining
1+ : Weak staining

Three of the luminal gene markers showed staining in the tumor transplants (Figure 8 and Table 5). Two of the As^{3+} (As #1 and As #4) and one Cd^{2+} (Cd #1) transformed cell line generated tumor showed no staining for KRT7, while the rest of the tumors showed a variable percentage of staining between 5 and 40%. When present, the intensity of the staining was judged to be between +2 and +3. All thirteen of the tumor samples showed staining for KRT19 with percentage intensity between 20 and 80% with strong staining localized to the periphery which contains the less differentiated areas of the tumor nests. The staining was localized to the less differentiated peripheral cells. CD24 staining was detected in 1 to 40% cells of the tumor with five of the tumors have no greater than 5% of the cells showing positive staining. The staining intensity for CD24 was between +2 and +3 for all the tumor samples and was present in the well-differentiated areas of the tumor only.
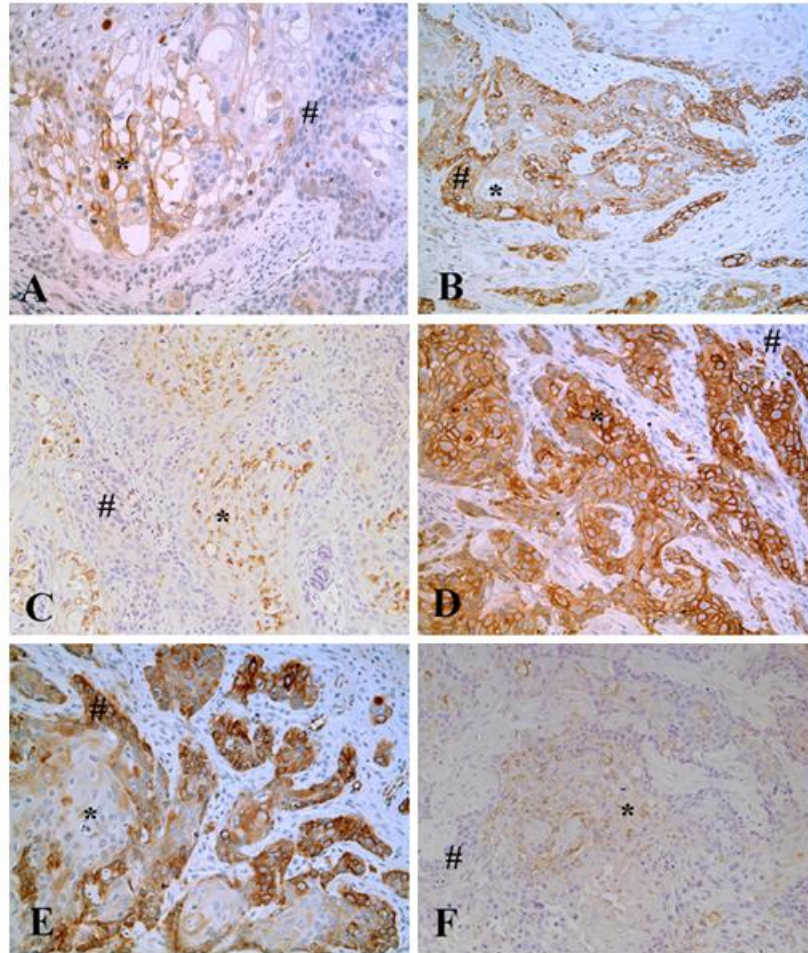
Figure 8. Immunohistochemical staining for luminal marker genes in the heterotransplant tumors generated from the As^{3+} and Cd^{2+}-transformed cell lines. (A-C) Staining of the As #3 cell line generated tumor for KRT7 (A), KRT19 (B), and CD24 (C). (A) There is strong staining in the well-differentiated cells in the center of the tumor nests (*), while the less differentiated peripheral cells (#) are negative for KRT7. (B) The tumor nests containing the well-differentiated cells (*) are weakly positive for KRT19, whereas there is strong staining for the less differentiated cells (#). (C) There is moderate to strong staining in for CD24 in the well-differentiated cells (*), as opposed to the less differentiated peripheral cells which are absent for CD24. (D-F) Staining of the Cd #3 cell line generated tumor for KRT7 (D), KRT19 (E), and CD24 (F). (D) There is strong staining in the well-differentiated cells in the center of the tumor nests (*) for KRT7, while the less differentiated peripheral cells (#) are negative. (E) The tumor nests containing the well-differentiated cells (*) are negative or weakly positive for KRT19, whereas there is strong staining for the less differentiated cells (#). (F) There is moderate to strong staining in for CD24 in the well-differentiated cells (*), whereas the less differentiated peripheral cells which are absent for CD24. The blue/purple color indicates the nuclei which are counterstained with hematoxylin and the brown color is indicative of the presence of the protein. Images are at a magnification of 200X.

Table 5. Expression and localization of luminal protein markers in different histological areas of the As^{3+} and Cd^{2+} tumor transplants.

Group	KRT7		KRT19		CD24		Well differentiated cells in the center of tumor nests			Peripheral less differentiated cells		
							KRT7	KRT19	CD24	KRT7	KRT19	CD24
	INT	%	INT	%	INT	%	INT	INT	INT	INT	INT	INT
As #1	-	0	3+	40	2-3+	40	-	1+	2-3+	-	3+	-
As #2	2+	10	3+	20	2-3+	30	2+	1+	2-3+	-	3+	-
As #3	2+	5	3+	30	2-3+	40	2+	1+	2-3+	-	3+	-
As #4	-	0	3+	80	2-3+	5	-	1+	2-3+	-	3+	-
As #5	3+	40	3+	40	2-3+	30	3+	1+	2-3+	3+	3+	-
As #6	2+	10	3+	40	3+	30	2+	0-1+	3+	-	3+	-
Cd #1	-	0	3+	40	2-3+	2	-	0-1+	2-3+	-	3+	-
Cd #2	3+	40	3+	40	2-3+	1	3+	1+	2-3+	3+	3+	-
Cd #3	3+	40	3+	40	2-3+	5	3+	0-1+	2-3+	3+	3+	-
Cd #4	3+	40	3+	30	2-3+	10	3+	0-1+	2-3+	3+	3+	-
Cd #5	2-3+	30	3+	40	2-3+	20	2-3+	0-1+	2-3+	2-3+	3+	-
Cd #6	2-3+	30	3+	40	2-3+	5	2-3+	-	2-3+	2-3+	3+	-
Cd #7	3+	40	3+	30	2-3+	10	3+	0-1+	2-3+	2-3+	3+	-

INT: Intensity of staining
% : % of cells staining for a marker
3+ : Strong staining
2+ : Moderate staining
2-3+ : Moderate to strong staining
1+ : Weak staining

Basal and luminal marker gene expression in the As^{3+} and Cd^{2+}-transformed

UROtsa cell lines and spheroids

The mRNA expression of basal and luminal markers was determined in the As^{3+} and Cd^{2+}-transformed cell lines and spheroids isolated from these cell lines. The results of this analysis for 9 basal markers showed that six markers were differentially expressed in the spheroids isolated from the As^{3+} transformed cell lines (Figure 9A). The expression level of KRT1 was below the level of detection in the As^{3+} transformed cell lines, but showed a significant increase in the spheroids. The expression levels of KRT6B, KRT6C, KRT14, and KRT16 were also significantly increased in the spheroids, whereas CDH3 expression was lower in the spheroids when compared to the As^{3+}-transformed cell lines. An identical analysis of the luminal marker genes in the As^{3+}-transformed cell lines and spheroids showed an increase in the expression levels of FABP4, FGFR3, and KRT20, whereas there was a decrease in the transcription factors FOXA1 and GATA3 (Figure 9B).

A Basal Marker Gene Expression in As^{3+}-Transformed Cell Lines and Spheroids

B Luminal Marker Gene Expression in As^{3+}-Transformed Cell Lines and Spheroids
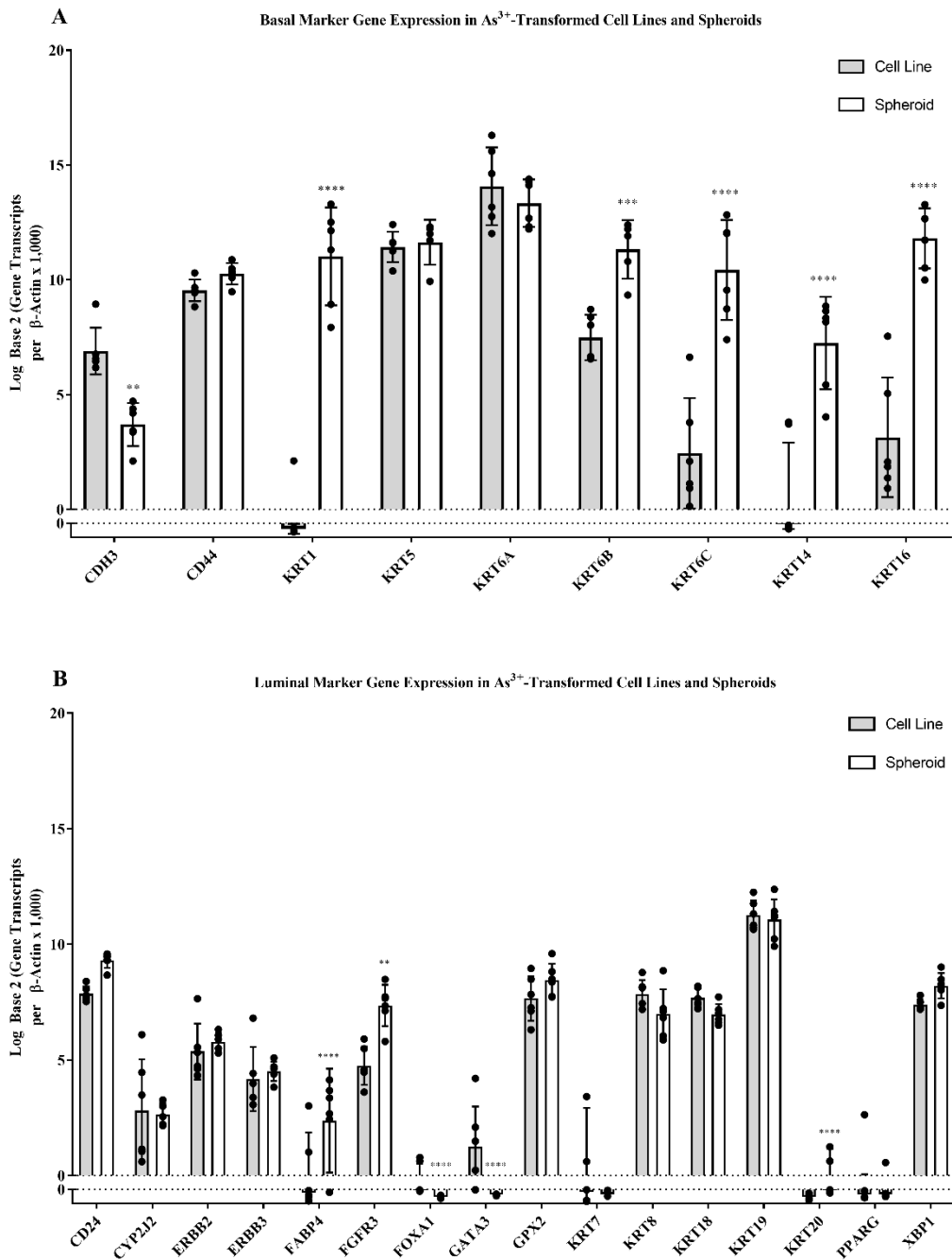
Figure 9. Gene expression analysis of basal and luminal marker genes in the As^{3+} transformed cell lines and their corresponding spheroids. Real-time RT-PCR analysis of basal (A) and luminal (B) marker genes in the As^{3+} transformed cell lines and spheroids. The analysis was done in triplicates and plotted as ± SD on a log base 2 scale per transcript of β-actin times 1,000. * indicates significantly different at p ≤ 0.05 from cell line. ** indicates significantly different at p ≤ 0.01 from cell line. *** indicates significantly different at p ≤ 0.001 from cell line. **** indicates significantly different at p ≤ 0.05 from cell line p ≤ 0.0001.

The mRNA expression of basal and luminal markers was determined in the Cd^{2+}-transformed cell lines and spheroids isolated from these cell lines. Similar results were obtained for the basal markers in the Cd^{2+}-transformed cell lines and spheroids with there being an increase in expression of KRT1, KRT6B, KRT6C, KRT14, and KRT16 and a decrease in the expression of CDH3 (Figure 10A). Analysis of the luminal marker genes in the Cd^{2+}-transformed cell lines and spheroids show an increase in the expression of FABP4 and decreases in expression of CYP2J2, FOXA1, GATA3, and KRT8 (Figure 10B). These results were similar to the ones obtained in the analysis of the expression of the As^{3+}-transformed spheroids compared to the transformed cell line with both showing an increase in the expression of FAPB4 and decreases in FOXA1 and GATA3. However, the As^{3+}-transformed cell line isolated spheroids showed significant increases in FGFR3 and KRT20, whereas the Cd^{2+}-transformed cell line isolated spheroids showed decreases in CYP2J2 and KRT8.
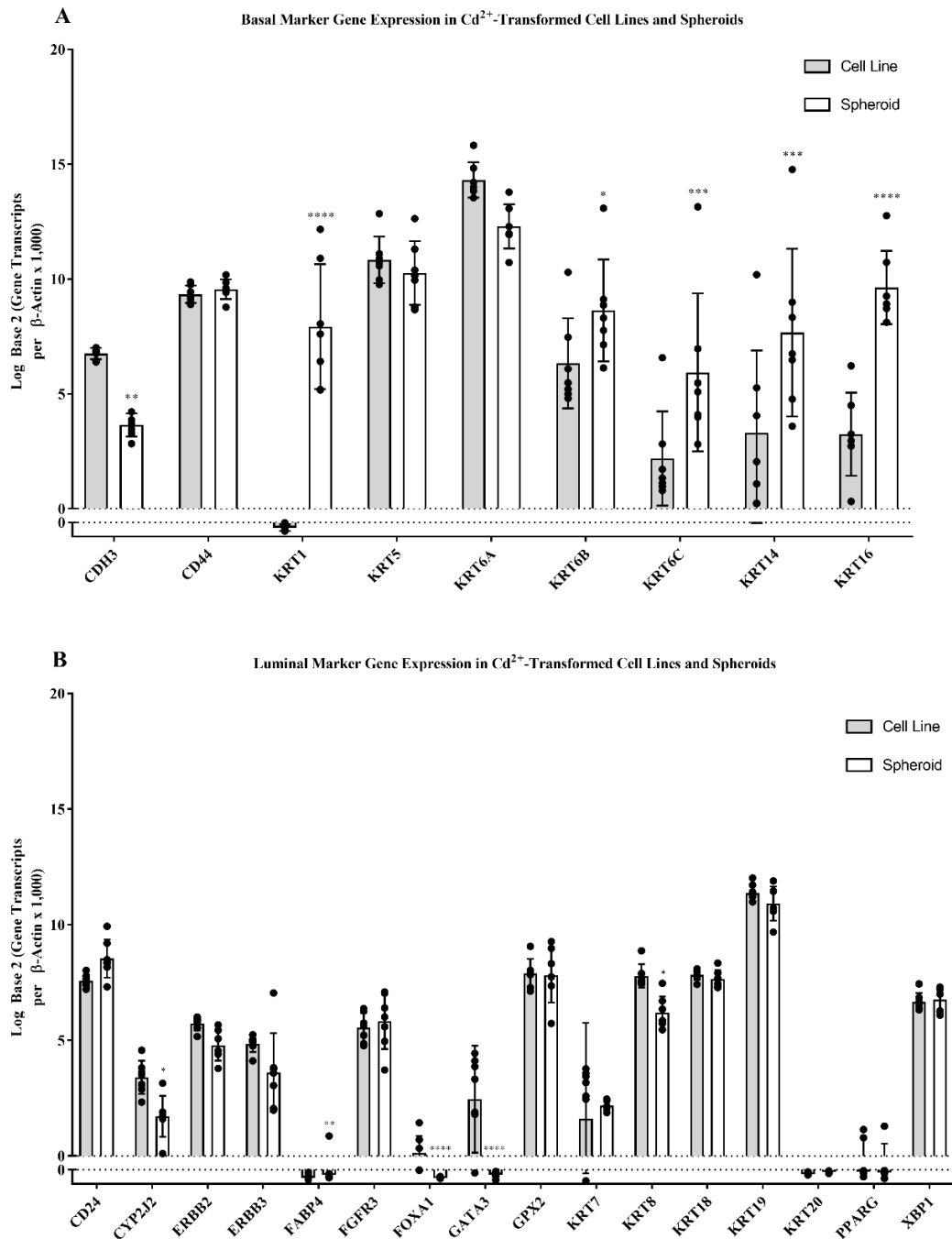
Figure 10. Gene expression analysis of basal and luminal marker genes in the Cd^{2+} transformed cell lines and their corresponding spheroids. Real-time RT-PCR analysis of basal (A) and luminal (B) marker genes in the Cd^{2+} transformed cell lines and spheroids. The analysis was done in triplicates and plotted as $\pm$ SD on a log base 2 scale per transcript of β-actin times 1,000. * indicates significantly different at $p \leq 0.05$ from cell line. ** indicates significantly different at $p \leq 0.01$ from cell line. *** indicates significantly different at $p \leq 0.001$ from cell line. **** indicates significantly different at $p \leq 0.05$ from cell line $p \leq 0.0001$.

Parental UROtsa cells produce nodules with areas of squamous differentiation

Although the tumors generated from the As^{3+} and Cd^{2+}-transformed cell lines produced prominent areas of focal squamous differentiation, it is unknown whether or not the parental UROtsa cells express these same areas of squamous differentiation when placed under *in vivo* conditions. Because this cell line is non-tumorigenic and does not produce tumors when injected into athymic mice, the parental UROtsa cell line and spheroids isolated from these cells were mixed with Corning® Matrigel® and subcutaneously injected under the skin of immune compromised (NCr-*nu*/*nu*) mice. After seven to ten days, the subcutaneous nodules were harvested and processed. Sections were H & E stained and examined for nests of cells (Figure 11A and 11B). It was found that these nests were composed of irregular shaped cells with branches or angular formations. The nodules from the parental UROtsa cells and spheroids were also stained for KRT5, to confirm an epithelial identity, and KRT6, a marker shown to identify areas of squamous differentiation in UROtsa tumor cells (Choi, et al., 2014). The cells stained positive for KRT5 (Figure 11C), whereas the staining for KRT6 (Figure 11D) was negative.
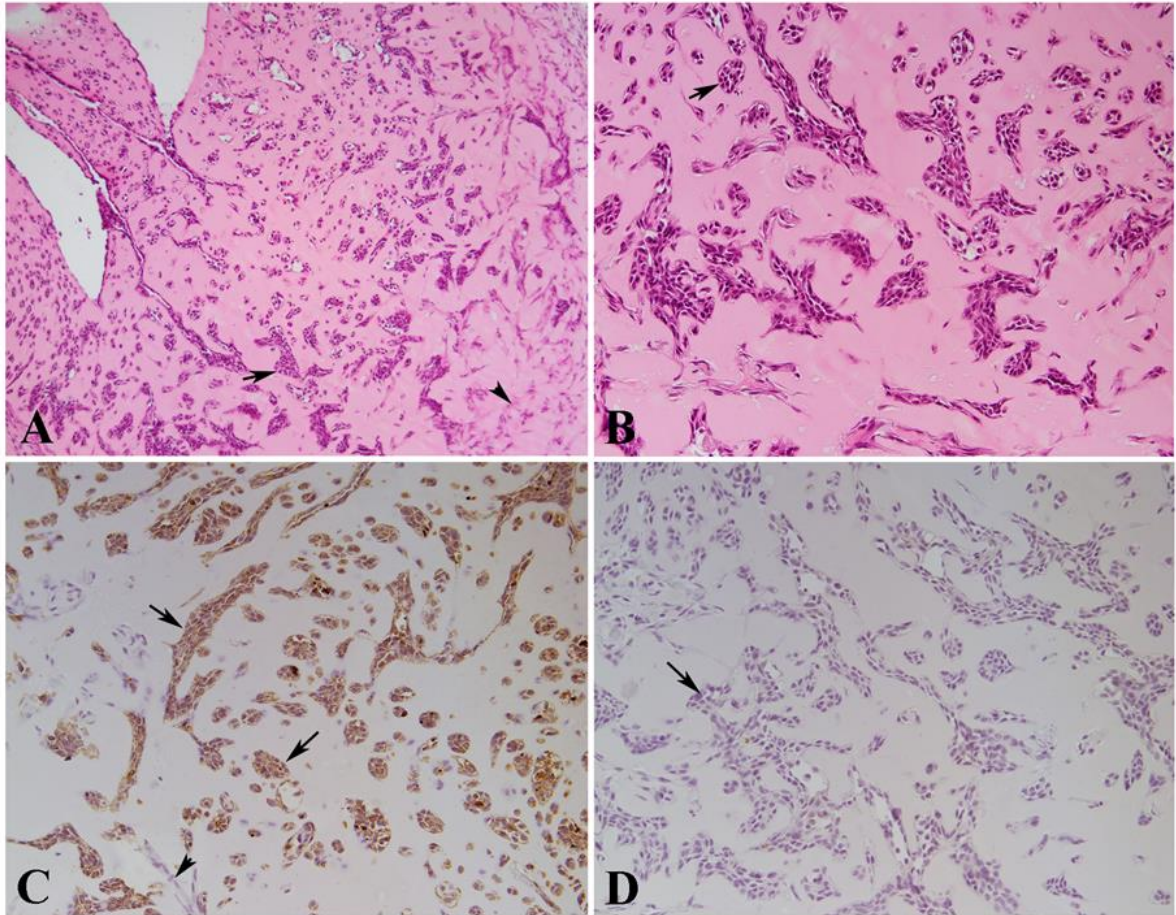
Figure 11. Histology and immunohistochemical staining of nodules formed by UROtsa cells injected with Matrigel® in immune compromised mice. Histology of a nodule formed by UROtsa cells at 100X magnification (A) and 200X magnification (B). Nests of epithelial cells of various shape and size seen in the Matrigel® (arrows). Many of the nests are irregular in shape with branches or angular formations, while a few nests are round or oval in shape, similar to the von Brunn's nests in the human bladder. Immunohistochemical staining for the basal marker genes KRT5 (C) and KRT6 (D). The epithelial nests (arrow) stain strongly for KRT5 and are absent for KRT6. The spindle stroma cells (arrowhead) are absent in staining for KRT5 and KRT6.

Basal and luminal marker gene expression in the parental UROtsa cell line and

spheroids

The expression of 9 basal and 16 luminal marker genes was assessed in the

parental UROtsa cell line and spheroids, which are generated from the parental cell line.

The results of the basal marker genes showed that six genes (KRT1, KRT6A, KRT6B,

KRT6C, KRT14, KRT16) were significantly elevated in the spheroids compared to the

parental cell line (Figure 12A). There was a significant decrease in the expression levels

of CDH3, CD44, and KRT5 in the parental spheroids when compared to the UROtsa cell

line. The basal marker gene expression results are similar to those found in the As^{3+} and

Cd^{2+}-transformed cell lines and spheroids, with both having increased expression levels

of KRT1, KRT6B, KRT6C, KRT14, and KRT16 and decreased expression of CDH3. For

the luminal marker genes, there was a significant increase in the expression of CD24,

FABP4, and KRT20 whereas there was a significant decrease in the expression of ten

genes (CYP2J2, ERBB3, FGFR3, FOXA1, GATA3, GPX2, KRT7, KRT8, KRT18, and

KRT19) (Figure 12B).
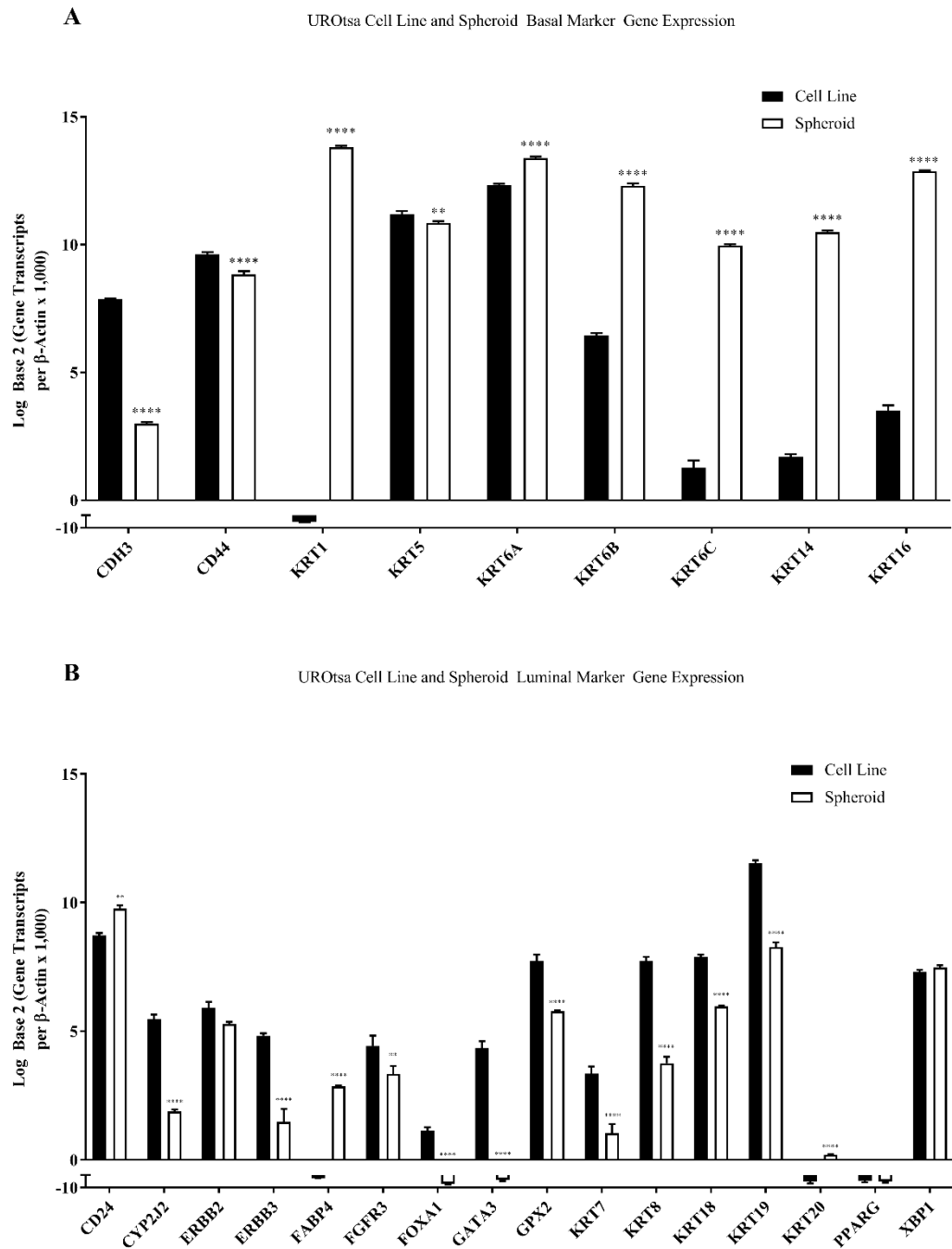
Figure 12. Gene expression analysis of basal and luminal marker genes in the parental UROtsa cell line and spheroids. Real-time RT-PCR analysis of basal markers (A) and luminal marker genes (B) in the parental UROtsa cell line and spheroids. The analysis was done in triplicates and plotted as ± SD on a log base 2 scale per transcript of β-actin times 1,000. * indicates significantly different at $p \leq 0.05$ from parental UROtsa cell line. ** indicates significantly different at $p \leq 0.01$ from parental UROtsa cell line. *** indicates significantly different at $p \leq 0.001$ from parental UROtsa cell line. **** indicates significantly different at $p \leq 0.0001$ from parental UROtsa cell line.

Expression of KRT17 and TP63 in the UROtsa Model System

In addition to the 25 MIBC marker genes identified by Choi and co-workers, research has found cytokeratin 17 (KRT17) is a basal-cell specific cytokeratin, which when highly expressed, identifies urothelial stem cells (He, et al., 2009). For this reason, we wished to know the expression of KRT17 in our As^{3+} and Cd^{2+} heterotransplant tumors and found high expression of KRT17 in the six As^{3+} and seven Cd^{2+} derived tumors (Figure 13A). Next, we analyzed protein expression via immunohistochemistry for KRT17 in the heterotransplant tumors and found strong staining in the well-differentiated areas of the tumor (*) and weak staining in the less differentiated cells (#) in the As^{3+}-derived tumor (Figure 13B). On the contrary, the Cd^{2+}-derived heterotransplant tumor showed weak staining in the well-differentiated cells (*) and strong staining in the less-differentiated cells (#) (Figure 13C). Lastly, we analyzed the mRNA expression of KRT17 in our parental UROtsa and six As^{3+} and seven Cd^{2+}-transformed cell lines and spheroids derived from these lines. KRT17 expression was found to be highly expressed in the cells lines and this expression was significantly increased in the respective spheroids (Figure 13D).

Previously, the UROtsa parent cell line was immortalized via the SV40 large T-antigen (Petzoldt, Leigh, Duffy, Sexton, & Masters, 1995). The effect of this virus is not known, but has shown to interact with p53 (Lilyestrom, Klein, Zhang, Joachimiak, & Chen, 2006), which in turn could influence the function of p53. For this reason, the mRNA expression of tumor protein 63 (TP63), a member of the p53 family (Wei, Zaika, & Zaika, 2011), was determined in the As^{3+} and Cd^{2+} UROtsa-derived tumors and was found to be moderately to highly expressed in all the tumors (Figure 13E).

Immunohistochemical analysis of TP63 in the heterotransplant tumors found moderate expression in the less differentiated areas of the tumor (#) with no staining in the well-differentiated areas of the tumor nests (*) in both the As #2 and Cd #3 cell line-derived tumors (Figure 13 F & G). Lastly, we analyzed mRNA expression of TP63 in our parental UROtsa and six As^{3+} and seven Cd^{2+}-transformed cells lines and derived spheroids and found high expression in the cell lines with significantly decreased expression in the parental UROtsa and As^{3+} spheroid (Figure 13H).
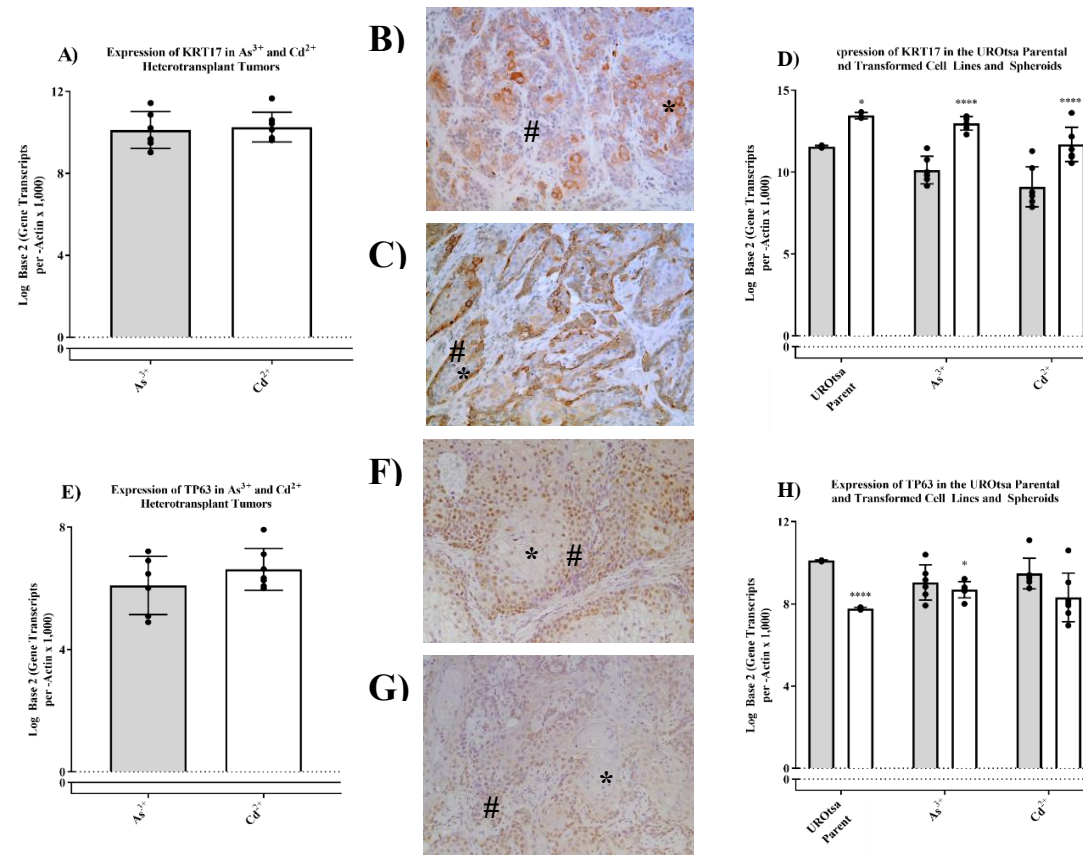
Figure 13. Expression of KRT17 and TP63 in the parental UROtsa and As^{3+} and Cd^{2+}-transformed UROtsa model. Real-time RT-PCR of KRT17 in the As^{3+} and Cd^{2+} tumors (A) and staining of the As #3 (B) and Cd #2 (D) cell line generated tumor for KRT17. mRNA expression of parental UROtsa, As^{3+} and Cd^{2+} cell lines and spheroids for KRT17 (D). Real-time RT-PCR of TP63 in the As^{3+} and Cd^{2+} tumors (E) and staining of the As #3 (G) and Cd #2 (H) cell line generated tumor for TP63. mRNA expression of parental UROtsa, As^{3+} and Cd^{2+} cell lines and spheroids (F). The analysis was done in triplicates and plotted as ± SD on a log base 2 scale per transcript of β-actin times 1,000. * indicates significantly different at p ≤ 0.05 from cell line. ** indicates significantly different at p ≤ 0.01 from cell line. *** indicates significantly different at p ≤ 0.001 from cell line. **** indicates significantly different at p ≤ 0.05 from cell line p ≤ 0.0001. * Indicates well-differentiated areas of the tumor. # indicates less differentiated areas of the tumor. The blue/purple color indicates the nuclei which are counterstained with hematoxylin and the brown color is indicative of the presence of the protein. Images are at a magnification of 200X.

Stability of the spheroid gene signature in the As^{3+} and Cd^{2+}-transformed and parental UROtsa cells

A second goal of this study was to determine the stability of the spheroid gene signature. This was accomplished by performing microarray analysis on triplicates of spheroids generated from a As^{3+}-transformed cell line (As #4) grown in regular cell culture flasks that promote cell attachment in serum-containing media, which is also used for the growth of the As #4 cell line. Triplicate samples were subjected to total RNA isolation when the spheroids reach confluency (passage 1) and at passages 4 (P4) and 8 (P8). The results showed that the gene expression signature of the spheroids returned to that of the As #4 parent cell line when placed under similar cell culture conditions. Of the initial 4,415 differentially expressed genes in the spheroids compared to the As #4 transformed cell line, by P1 70.9% of those genes had returned to the level of expression of the As #4 cell line. This trend continued at P4 and P8 with 89.8% and 95.7%, respectively, of the differentially expressed genes returned to the level of the As #4 transformed parental cell line.

The growth and isolation of the spheroids utilizes low attachment plastic culture vessels with serum-free growth media, while the parental cell lines are grown in serum-containing media in vessels that promote cell attachment. It was demonstrated that by growing the spheroids in serum-containing growth media in vessels promoting attachment, the gene signature returned to that of the As #4 parental cell line. Because of these results, we wished to know if the spheroids from the As^{3+} and Cd^{2+}-transformed cell line and parental UROtsa cell line would retain their gene signatures if they were cultured in serum-free media in adherent culture vessels. To do this, the spheroids were cultured in

serum-free growth media in vessels that promoted cell attachment and isolated at P1, P4, and P8.

Analysis of the 25 MIBC marker genes in the As #4 transformed cell line, spheroid, and passages shows that 84% of the genes are differently expressed in the spheroid compared to the parental As #4 transformed cell line. This trend is continued in the spheroids placed in regular attachment flasks with serum-free media; the percent of differently expressed genes at P1 and P4 is 72, while the percentage increases to 84% at P8 (Figure 14).
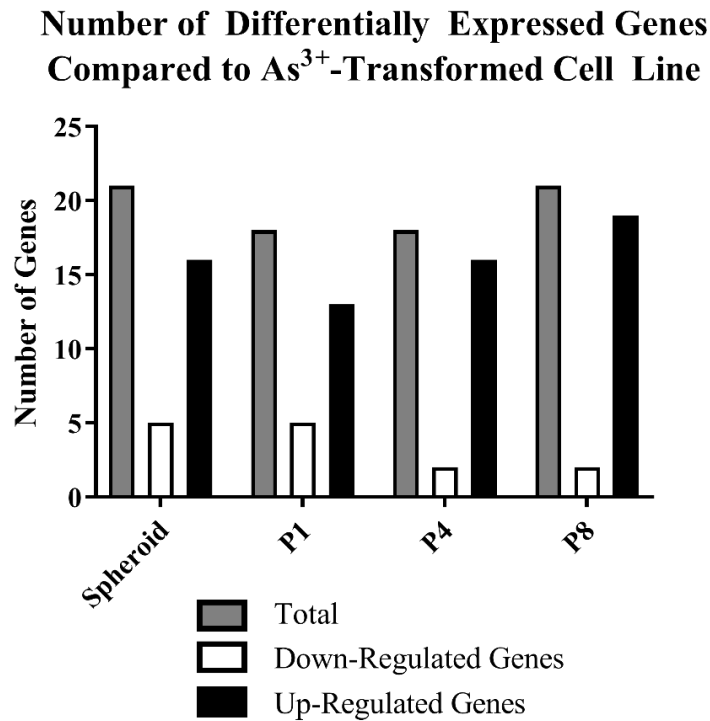
Number of Differentially Expressed Genes Compared to As^{3+}-Transformed Cell Line

Figure 14. Number of differentially expressed genes in the spheroid and passages compared to the As^{3+}-transformed cell line when cultured in serum-free conditions. The total number of genes and the number of down- and up-regulated is plotted for the spheroids and passages cultured in serum-free media.

The mRNA expression of the basal markers showed an initial decrease in expression of CDH3 in the spheroid, but increased expression in the passages (Figure 15A). CD44 expression showed an increase in the spheroid, but no difference between

70

the parental transformed cell line and the passages (Figure 15B). The expression of KRT1 was increased in the spheroid, returned to baseline levels in P1 and P4, but saw another increase in P8 (Figure 15C). KRT5 expression was increased in the spheroids and all three passages (Figure 15D), whereas KRT6A showed the opposite expression and was found to be decreased in all of the samples compared to the As #4 transformed cell line (Figure 15E). The expression of KRT6B was increased only in the spheroids (Figure 15F), while KRT6C expression saw increases across all samples (Figure 15G). KRT14 showed a slight induction in the spheroid, but a great induction in the passages (Figure 15H). Lastly, KRT16 expression was increased in the spheroid, returned to similar levels in P1 and P4, but showed an induction of expression by P8 (Figure 15I).

Analyzing the mRNA expression of the luminal markers found increased levels of CD24, CYP2J2, ERbβ2, and ERbβ3 (Figure 16A-D) in the spheroids and all three passages. There was only an increase in FAPB4 in the spheroid (Figure 16E). FGFR3 expression was increased in all the samples (Figure 16F), whereas FOXA1 showed opposite expression, being decreased in all the samples (Figure16G). There was no change in the expression of the transcription factor GATA3 in the spheroid and P4, however there was found to be a decrease in P1 and increase by P8 (Figure 16H). GPX2 expression was found to be increased in the spheroid, P1, P4, and P8 (Figure 16I). Conversely, KRT7 expression was decreased in the spheroid and passages compared to the As #4 transformed cell line (Figure 16J). KRT8 expression was increased in the spheroid and all three passages (Figure 16K). There was increased expression of KRT18 in P4 and P8 (Figure 16L), whereas there was an increase in expression of KRT19 in the spheroid and all three passages (Figure 16M). KRT20 expression was found to be

increased in the spheroid, returned to baseline in P1 and P4, but increased again in P8 (Figure 16N). The receptor PPARγ saw increased expression in the passages (Figure 16O) and the expression of XBP1 was decreased in the spheroid, but levels returned to baseline by P1 and was found to be increased in P4 and P8 (Figure 16P).
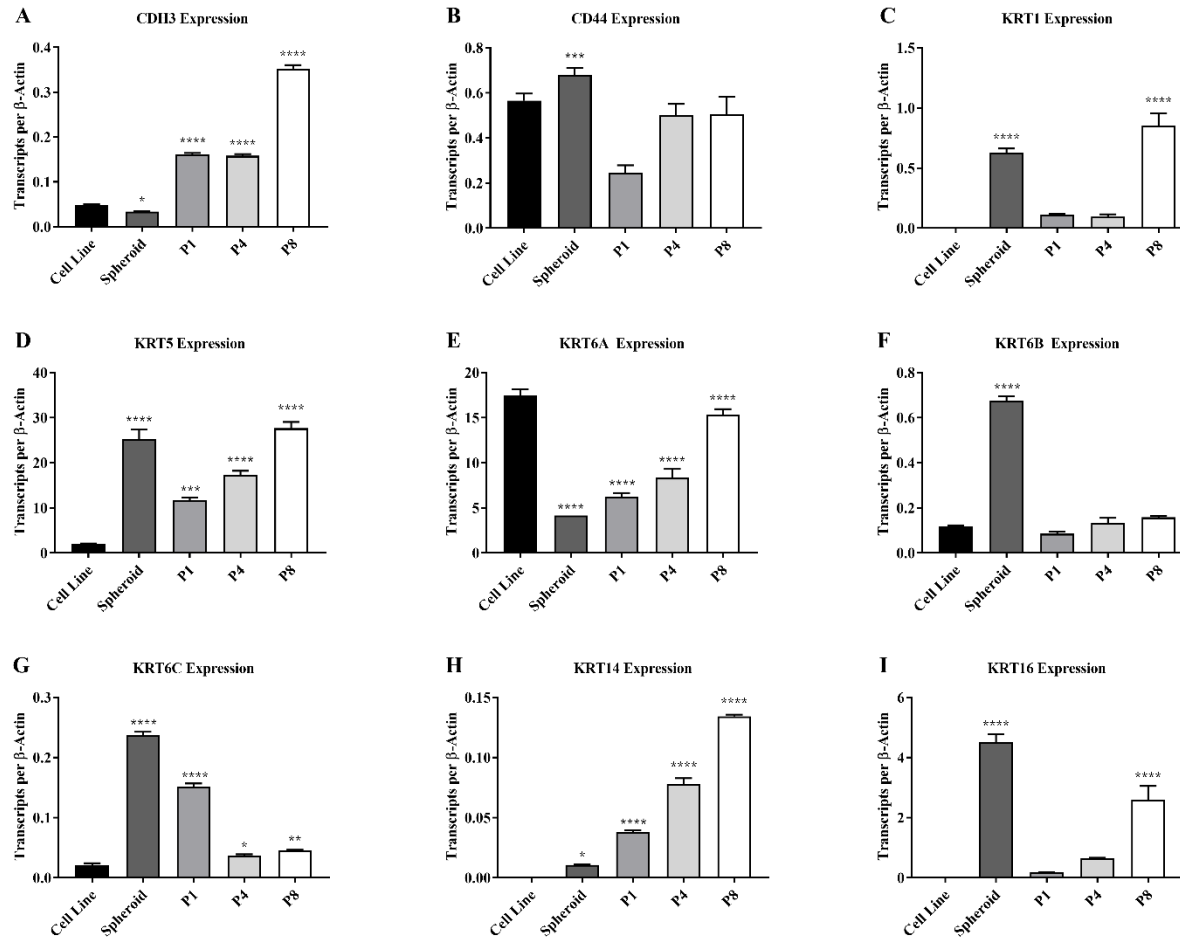
Figure 15. Gene expression analysis of basal marker genes in the As³⁺-transformed cell line, spheroids, and passages. (A-I) Real-time RT-PCR analysis of basal markers marker genes in the As³⁺-transformed cell line, spheroids, and serial passages. The analysis was done in triplicates and plotted as ± SEM per transcript of β-actin.

73
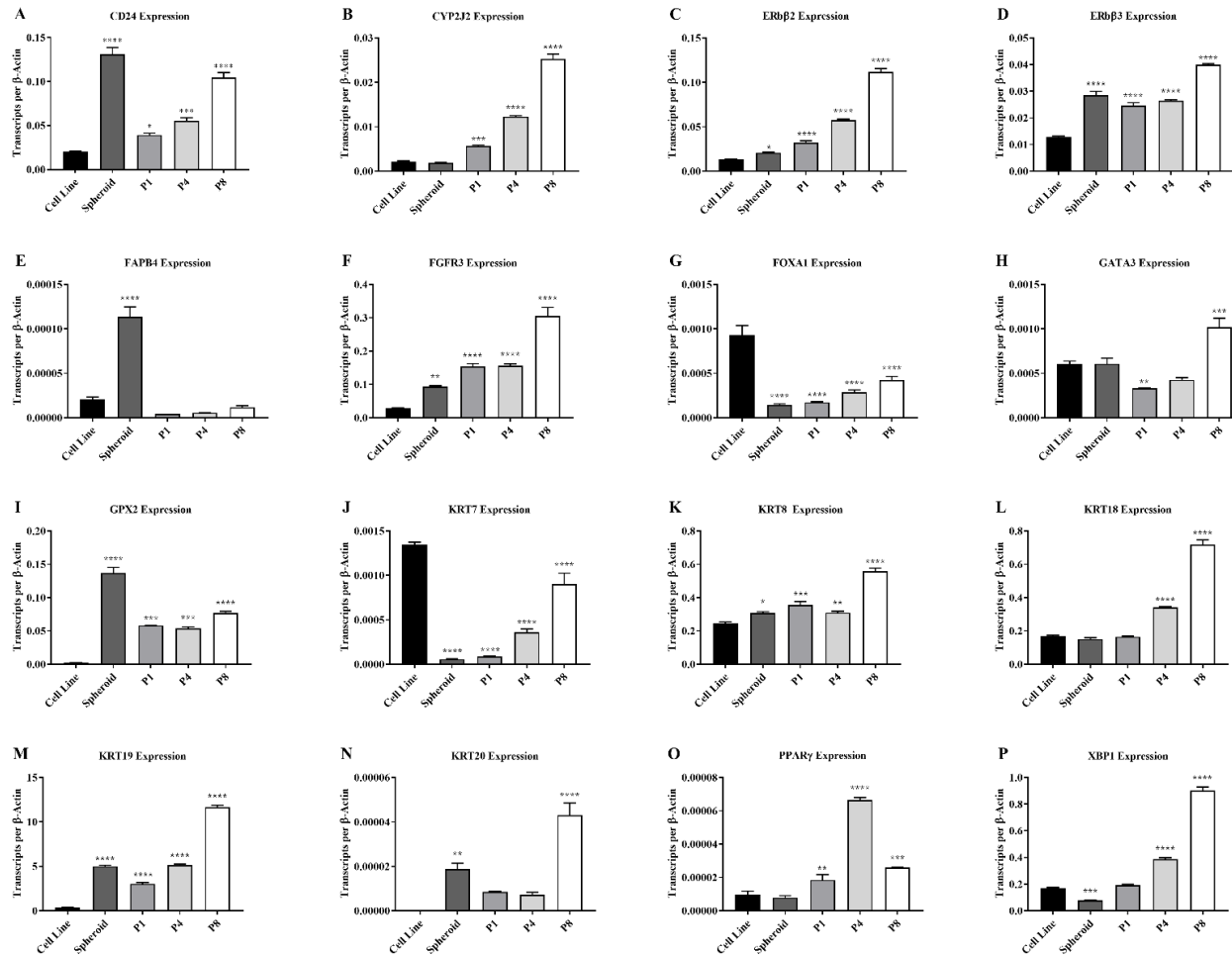
Figure 16. Gene expression analysis of luminal marker genes in the As^{3+}-transformed cell line, spheroids, and passages. (A-P) Real-time RT-PCR analysis of luminal marker genes in the As^{3+}-transformed cell line, spheroids, and serial passages. . The analysis was done in triplicates and plotted as ± SEM per transcript of β-actin.

Analysis of the 25 MIBC marker genes in the Cd #4 transformed cell line, spheroid, P1, P4, and P8 grown in serum-free cell culture media showed that 84% of the genes are differentially expressed in the Cd #4 transformed cell line compared to the spheroid. This high percentage of differentially expressed genes continues in the passages where 92% of the genes are differentially expressed in P1, 72% in P4, and 68% in P8 (Figure 17). These results are similar to what was seen in the As #4 serum-free culture analysis with a majority of the genes being differentially expressed throughout the spheroid and subsequent passages.
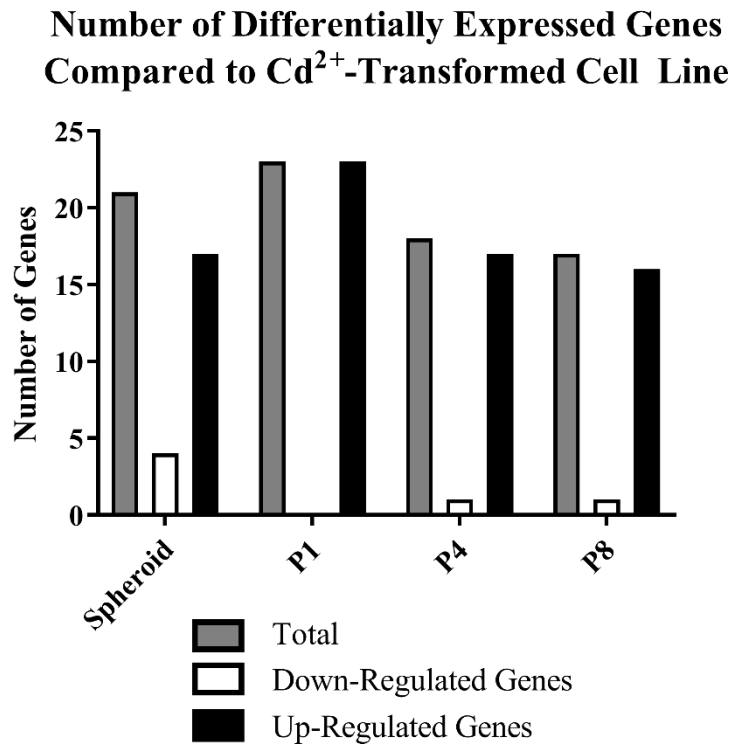
Figure 17. Number of differentially expressed genes in the spheroid and passages compared to the Cd^{2+}-transformed cell line when cultured in serum-free conditions. The total number of genes and the number of down- and up-regulated is plotted for the spheroids and passages cultured in serum-free media

While the overall number of differentially expressed genes is similar between the As #4 and Cd #4 data sets, the Cd #4 gene expression analysis shows a higher ratio up-regulated to down-regulated differentially expressed genes.

The mRNA expression of the basal subtype specific marker genes showed an initial decrease in CDH3 in the spheroid followed by increased expression in the three passages (Figure 18A). The expression of CD44 significantly increased in the passages (Figure 18B), whereas KRT1 expression increased in the spheroid and returned to baseline by P4 (Figure 18C). KRT5 expression was increased in the spheroids, P1, P4, and P8 (Figure 18D). The three keratin 6 isoforms (KRT6A, 6B, and 6C) all showed increases in the spheroid, but gradually returned to similar expression levels of the Cd #4 transformed cell line by P8 (Figure 18E-G). KRT14 expression was increased in the spheroid and all three passages compared to the Cd #4 transformed cell line (Figure 18H), whereas KRT18 showed an increase in expression in the spheroid, but decreased in the passages and by P8 returned to expression levels of the Cd #4 cell line (Figure 18I). The expression of CDH3 and KRT5 was similar in the As #4 and Cd #4 data sets, whereas KRT1 and KRT16 expression saw increases in expression in the As #4 model, but decreases in expression in the Cd #4 samples.

The luminal gene marker expression in the Cd #4 spheroid and passages showed an increase of expression in CD24 in the samples (Figure 19A), whereas CYP2J2 had a decrease in expression in the spheroid, but showed a significant induction in the passages (Figure 19B). There was no change in expression of ERbβ2 in the spheroid, but an increase in expression in the passages (Figure 19C). ERbβ3 expression was increased in all samples (Figure 19D), however, FAPB4 was only induced in the spheroid (Figure

19E). The expression of FGFR3 was increased relative to the Cd #4 cell line, with the exception being P4 (Figure 19F). The transcription factor FOXA1 expression was decreased in the spheroid, P4, and P8, while increased in P1 (Figure 19G). GATA3 expression was increased in the spheroids and subsequent passages (Figure 19H). The expression of GPX2 was induced in the spheroid, P1, and P8 (Figure 19I). KRT7 expression was increased in P1 and P4, but returned to baseline levels by P8 (Figure19J). The expression of KRT8, KRT18, and KRT19 was increased in the spheroids and passages (Figure 19K-M). KRT20 expression was induced in the spheroid and returned to baseline levels (Figure 19N), whereas PPARγ was increased in the passages (Figure 19O). Lastly, the expression of XBP1 initially decreased in the spheroid, but was induced in the passages (Figure 19P). The expression of the luminal marker genes CD24, ERbβ3, FAPB4, KRT8, KRT19, and PPARγ showed similar expression levels of the spheroids and passages compared to the As #4 or Cd #4 transformed cell line.
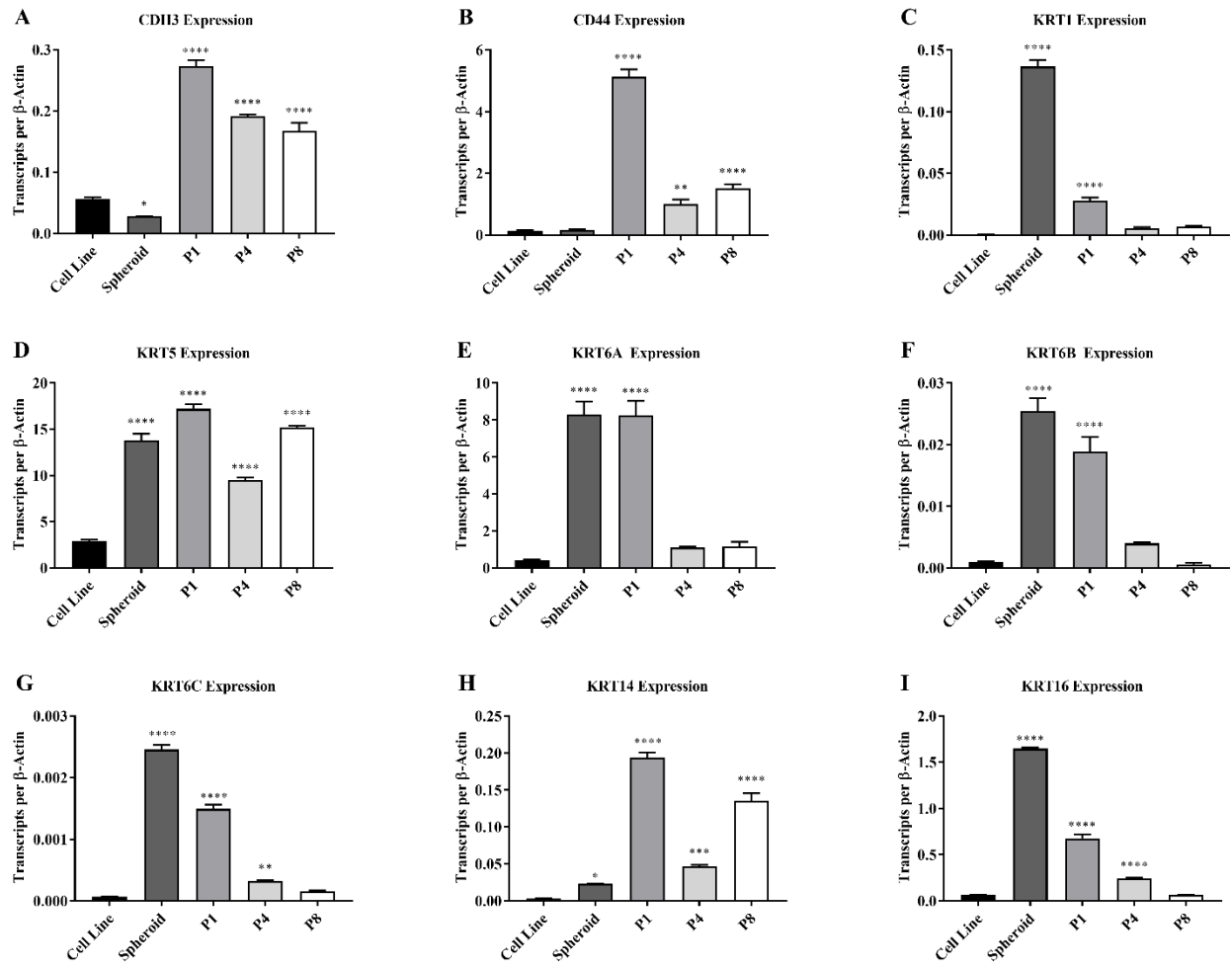
Figure 18. Gene expression analysis of basal marker genes in the Cd^{2+}-transformed cell line, spheroids, and passages. (A-I) Real-time RT-PCR analysis of basal markers marker genes in the Cd^{2+}-transformed cell line, spheroids, and serial passages. The analysis was done in triplicates and plotted as ± SEM per transcript of β-actin.
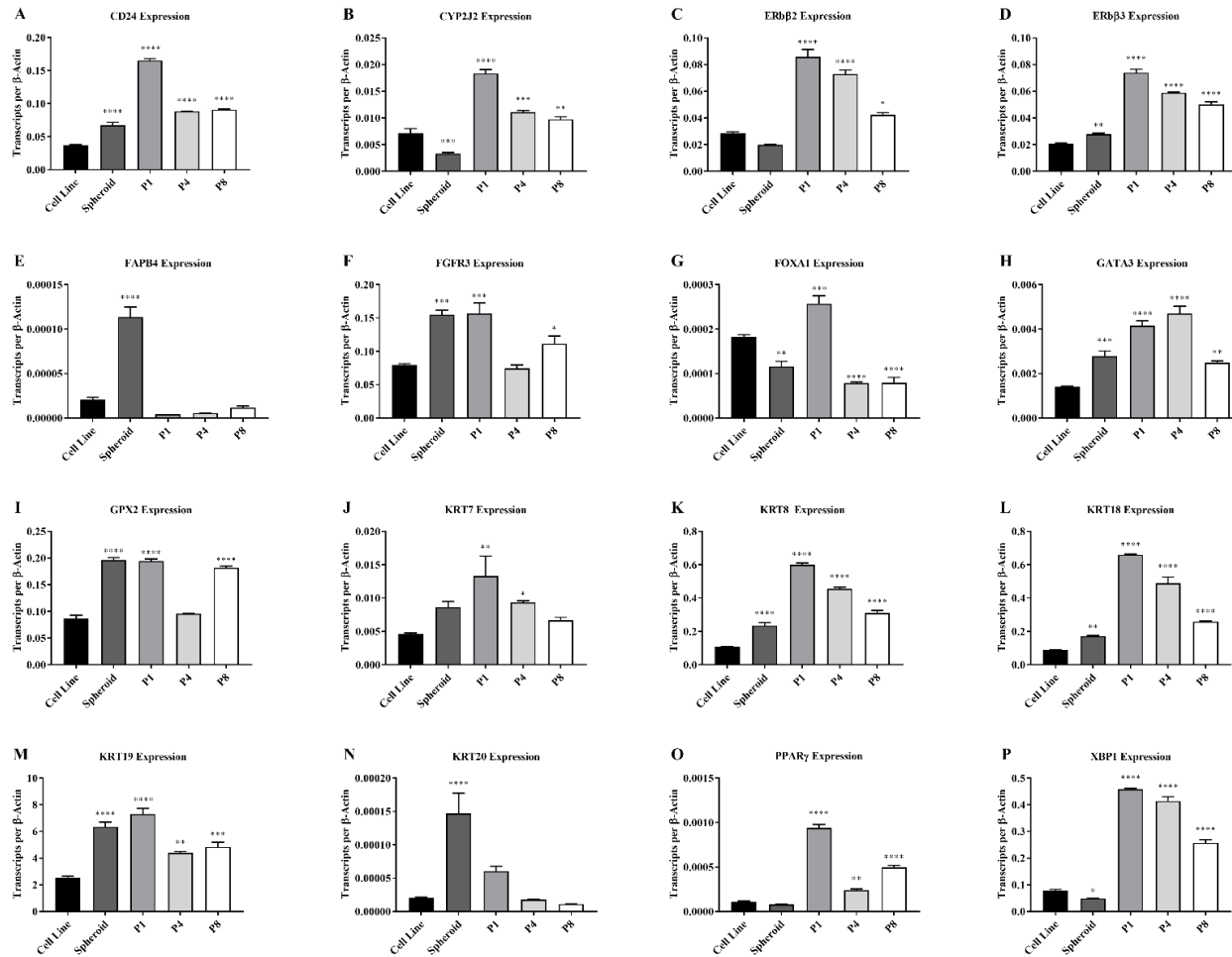
Figure 19. Gene expression analysis of luminal marker genes in the Cd^{2+}-transformed cell line, spheroids, and passages. (A-P) Real-time RT-PCR analysis of luminal marker genes in the Cd^{2+}-transformed cell line, spheroids, and serial passages. . The analysis was done in triplicates and plotted as ± SEM per transcript of β-actin.

The mRNA expression analysis of the 25 MIBC marker genes in the UROtsa cell line, spheroid, and passages cultured in serum-free media showed a great percentage of the genes being differentially expressed compared to the parental cell line at the spheroid and each passage. Analysis found 84% of the genes were differentially expressed in the spheroid and P1, 88% in P4 and 76% in P8 (Figure 20). These trends align with the As #4 and Cd #4 serum-free cultured spheroids and passages. However, unlike those data sets, the UROtsa expression analysis showed a greater ratio of down-regulated to up-regulated genes.

Number of Differentially Expressed Genes Compared to UROtsa Cell Line
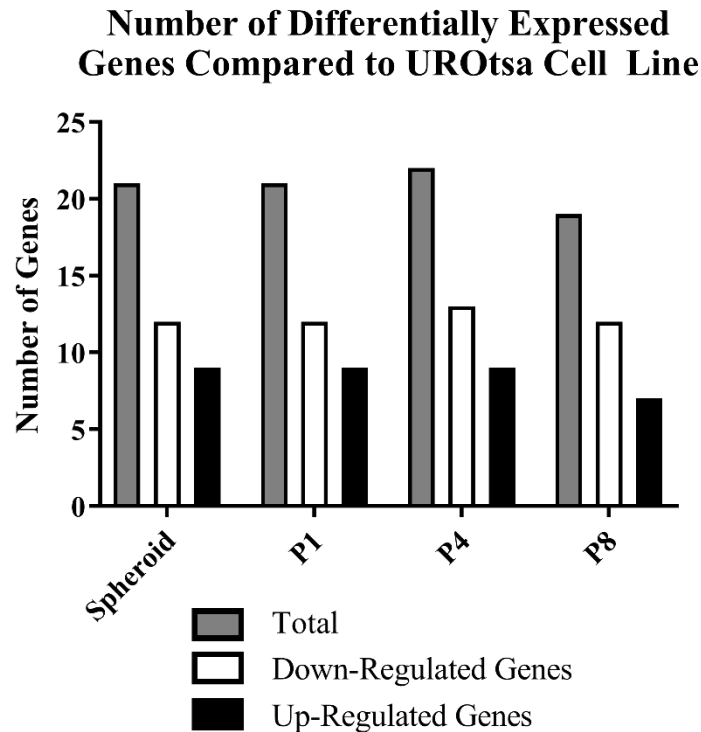
Figure 20. Number of differentially expressed genes in the spheroid and passages compared to the UROtsa cell line when cultured in serum-free conditions. The total number of genes and the number of down- and up-regulated is plotted for the spheroids and passages cultured in serum-free media.

Analysis of the basal specific marker genes of MIBC found decreased expression levels of CDH3 in the spheroid and passages (Figure 21A). The expression of CD44 was decreased in the spheroid and increased in P1 and P4 (Figure 21B). KRT1 expression was greatly induced in P4 and P8 (Figure 21C) and KRT5 showed an increase in expression across all the samples compared to the UROtsa cell line (Figure 21D). The expression of the keratin isoforms (KRT6A, 6B, and 6C) was increased in all the spheroids and passages, except for P1 in KRT6A (Figure 21E-G). The expression of KRT14 was induced in the passages (Figure 21H). Lastly, KRT16 expression was increased in the spheroid and P1, but decreased in P4 and P8 (Figure 21I). The expression of CDH3 was opposite of what was seen in the As #4 and Cd #4 data sets, however the expression of KRT5 and KRT14 was alike in all three.

Analysis of the mRNA expression of the luminal MIBC marker genes found expression of CD24, CYP2J2, and ERbβ2 to be decreased in the spheroids and passages (Figure 22A-C). The expression of ERbβ3 was increased in the spheroid and P4, but decreased in P1 (Figure 22D). FABP4 expression was induced in the spheroid and decreased in P1 and P4 (Figure 22E). The expression FGFR3 was decreased in the spheroids and increased in P1 (Figure 22F). The expression of FOXA1 and GATA3 was decreased in the spheroids and passages (Figure 22G-H), whereas GPX2 expression was increased in all the samples (Figure 22I). KRT7, KRT8, and KRT18 expression was decreased in the spheroids and passages (Figure 22J-L). The expression of KRT19 was decreased in P4 and P8 (Figure 22M), whereas expression of KRT20 was induced in the spheroid and P1, but returned to similar levels of the UROtsa cell line by P4 (Figure 22N). Lastly, the expression of PPARγ and XBP1 were decreased in the spheroid

and subsequent passages (Figure 22O-P). The expression of FABP4 and GPX2 in the UROtsa serum-free culture model was similar to the results seen in the As #4 and Cd #4 data, while the expression of CD24, KRT8, and XBP1 showed opposite results.
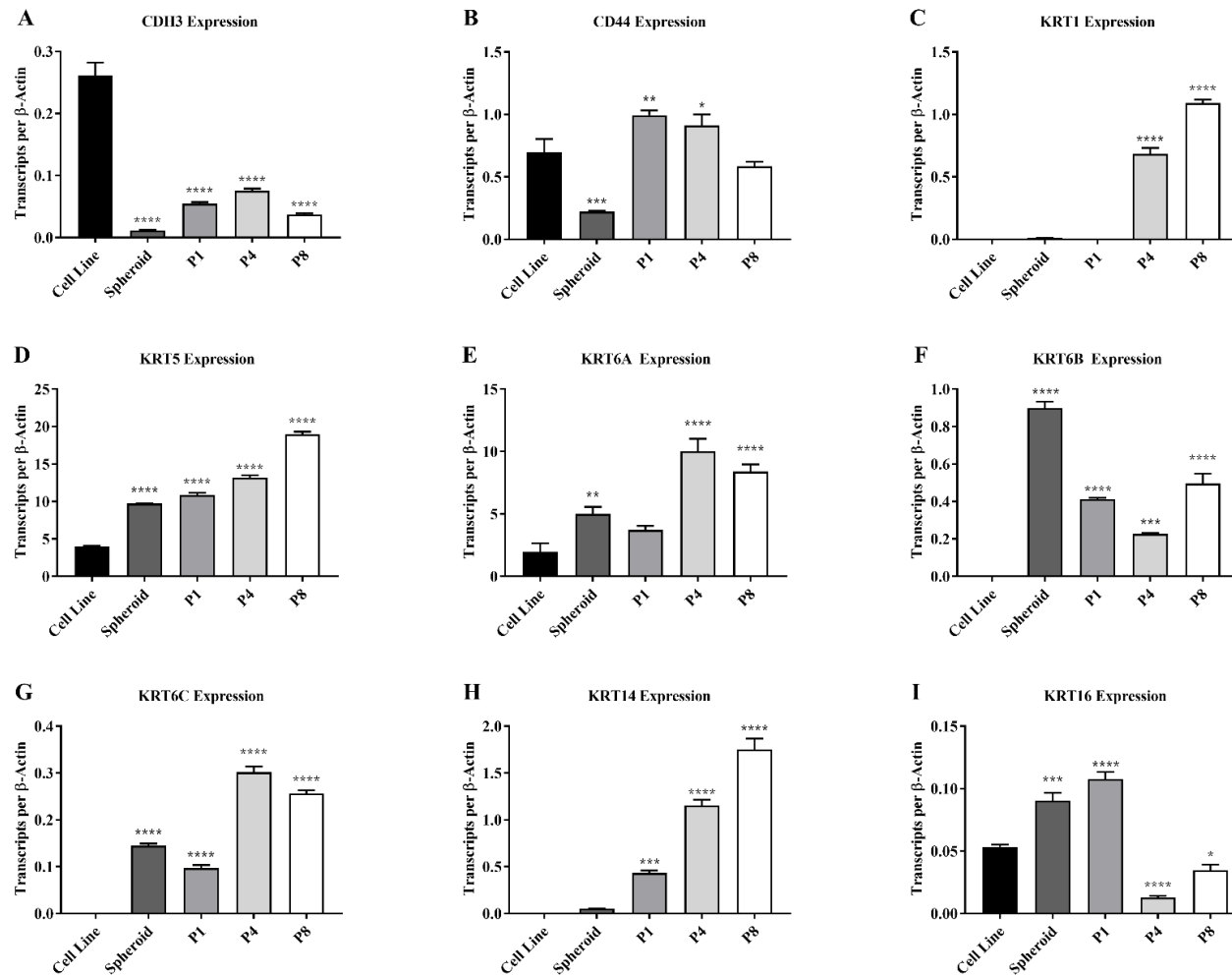
Figure 21. Gene expression analysis of basal marker genes in the parental UROtsa cell line, spheroids, and passages. (A-I) Real-time RT-PCR analysis of basal markers marker genes in the parental UROtsa cell line, spheroids, and serial passages. The analysis was done in triplicates and plotted as ± SEM per transcript of β-actin.
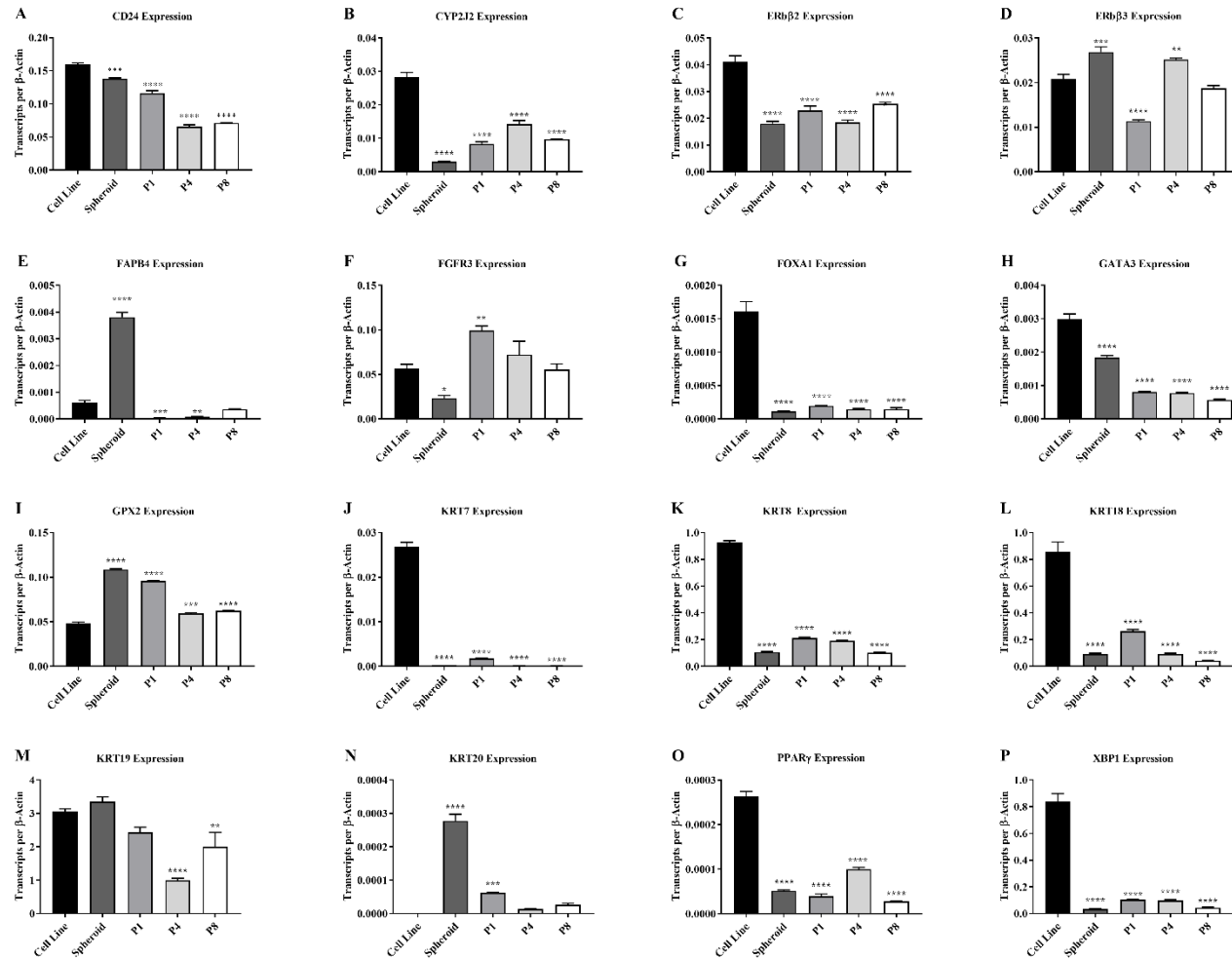
Figure 22. Gene expression analysis of luminal marker genes in the parental UROtsa cell line, spheroids, and passages. (A-P) Real-time RT-PCR analysis of luminal marker genes in the parental UROtsa cell line, spheroids, and serial passages. . The analysis was done in triplicates and plotted as ± SEM per transcript of β-actin

CHAPTER IV

DISCUSSION

Our laboratory has determined that the tumor transplant generated from the As^{3+} and Cd^{2+}-transformed UROtsa cells display a basal gene expression pattern identified by a recent study (Choi, et al., 2014) through two different approaches. First the expression of mRNA for the 9 basal and 16 luminal marker genes from the tumors derived from the six isolates of the As^{3+} and seven isolates of the Cd^{2+}-transformed UROtsa cells was compared to the 73 primary MIBCs selected for analysis in the study by Choi and coworkers (Choi, et al., 2014). The results showed that unsupervised hierarchical clustering of the samples found that the As^{3+} and Cd^{2+} tumors demonstrated a strong identify with the basal subtype of MIBCs. These results were supported by comparing the mRNA expression levels of the basal and luminal marker genes in the tumors derived from the six isolates of As^{3+} and seven isolates of Cd^{2+}-transformed cells and finding an elevated expression of the basal compared to the luminal marker genes.

Despite the supporting results of the unsupervised hierarchical clustering and comparison of mRNA expression levels of the marker genes, concerns regarding the high expression of the keratins in the basal and luminal subtypes and the multiple transcription factors associated with the luminal subtype. Because of their association with the cytoskeleton, the keratins may have high levels of expression and transcription factors are known to exert their influence at low expression levels. However, two of the keratins

associated with the luminal subtype (KRT7 and KRT20), showed only modest and no expression, respectively.

The final piece of evidence that the As^{3+} and Cd^{2+}-transformed derived tumors show characteristics of the MIBC basal subtype is the immunohistochemical expression of the basal and luminal markers. Besides CDH3, all of the tumors showed a strong staining for the other basal markers. Opposed to the high expression of the basal markers, only three luminal markers showed staining in the tumor transplants (CD24, KRT7, and KRT19). Therefore, the tumors generated from the As^{3+} and Cd^{2+}-transformed parental UROtsa cells display expression patterns that aligns with the basal subtype of MIBCs.

The characterization of the UROtsa-derived tumors as the basal subtype of MIBC could be influenced by multiple factors. First, because of the generation of the tumors in athymic mice, there is limited influence of immune cells on the tumors, which interrupts the interaction of the stroma and tumor. Next, the UROtsa parent cell line was immortalized via the SV40 large T-antigen (Petzoldt, Leigh, Duffy, Sexton, & Masters, 1995). The effect of this virus is not known, but has shown to interact with p53 (Lilyestrom, Klein, Zhang, Joachimiak, & Chen, 2006), which in turn could influence the function of p53. For this reason, the expression of p63, a member of the p53 family (Wei, Zaika, & Zaika, 2011), was determined in the UROtsa-derived tumors and was found to be expressed in all the tumors.

The expression of mRNA for the basal and luminal marker genes was also analyzed in the As^{3+} and Cd^{2+} transformed cell lines and spheroids generated from each of the six As^{3+} and seven Cd^{2+} cell lines. These cells lines had expression patterns that identified the most with the basal gene signature and this identity was increased in the

spheroids isolated from the cell lines. The expression of KRT1, KRT6B, KRT6C, KRT14, and KRT16 was increased in the spheroids compared to the As^{3+} and Cd^{2+}-transformed cell lines. These basal gene markers were also upregulated in the tumors generated from the transformed cells.

The next part of this study looked at the mRNA expression of the basal and luminal marker genes in the parental UROtsa cell line and the spheroids isolated from these cells. The expression levels were compared to the transformed cell lines, tumors from these cell lines, and the MIBCs. The results showed that the spheroids from the parental UROtsa cells showed increased expression of all the basal keratins (KRT1, KRT5, KRT6A, KRT6B, KRT6C, KRT14, and KRT16), whereas there was decreased expression of CDH3 and CD44. The increased of expression of five of these six keratins was seen in the spheroids isolated from the transformed cells and tumors derived from these cell lines along with the decreased expression of CDH3. With the overlapping increase of five out of the six basal keratins in the parental UROtsa and As^{3+} and Cd^{2+} transformed cell line derived spheroids, this suggests that these basal keratins may be markers of urinary carcinoma with characteristics of squamous differentiation. The results also suggests that the spheroids isolated from the parental UROtsa cells undergo transformation with As^{3+} and Cd^{2+} and gain the ability to form tumors in aythmic mice.

The study then shifted focus and examined if the gene signature seen in the spheroids could be maintained once the spheroids were placed back in conditions used to grow the original cell line. The growth and isolation of the spheroids utilizes low attachment culture vessels with serum-free growth media, in contrast to the parental cell lines, which are grown in vessels promoting attachment with serum-containing growth

media. Microarray analysis data found that the gene signature of the spheroids isolated from one of the As^{3+}-transformed cell lines (As#4) reverted back to that of the original cell line. Upon reaching confluency, over 70% of the differentially expressed genes were no longer expressed and seven more serial passages showed that 95% of the genes were no longer differentially expressed. These results suggests that a culture environment of serum-containing media does not allow for differentiation of our UROtsa model system.

In addition, a limited analysis of the 25 MIBC marker genes of the same experimental cell culture set-up, except cultured in serum-free media, found an expression profile for the As #3, Cd #3, and parental UROtsa cells to be different when comparing the cell line to the spheroids and serial passages. The As #3 spheroid and serial passages saw increases in the basal markers KRT5 and KRT14, which are markers of the basal cell compartment of the bladder (McConkey, Choi, Ochoa, & Dinney, 2016). The luminal markers Erb-β2 and Erb-β3 showed increases in the spheroids and serial passages compared to the cell line, which suggests an increase in proliferation due to the heterodimerization of these co-receptors and subsequent signaling of the PI3K pathway (Holbro, et al., 2003). Furthermore, a knockout of FOXA1, a DNA-binding protein that plays a role in metabolism and interactions with hormones, has resulted in the development of keratinizing squamous metaplasia in mice (Shuman, et al., 2017). Lastly, the results showed an increase in glutathione peroxidase 2 (GPX2), which suggests an increase in proliferation and ROS (Naiki, et al., 2017). Taken altogether, the As #3 unique gene signature shows increased levels of growth and proliferation due to increased expression of basal cells and reactive oxygen species furthering the development of squamous differentiation and urinary carcinoma.

The Cd #3 cell line showed decreases of expression in KRT5 and KRT14, similar to those of the As #3 cell line. The luminal marker gene GATA3 was increased in the spheroids and serial passages, which could be indicative of decreased invasion and progression (Li, et al., 2014). Also increased in expression was the transcription factor X-box binding protein 1 (XBP1), which has been implicated in the unfolded protein response and shown to lead to an increase in innate immune response and a potent cytotoxic T-lymphocyte engagement (Overley-Adamson, et al., 2014). Taken together, there may be a unique gene signature that is less invasive and a less progressive form of urinary carcinoma.

The parental UROtsa spheroids and serial passages showed a decrease in expression of P-cadherin (CDH3), which has been linked to muscle-invasive disease (Mandevilla, et al., 2008) and increases in KRT5 and KRT14. Similar to the As #3 cell line, spheroids, and serial passages, the parental UROtsa model showed a decrease in expression of FOXA1 and an increase in GPX2. However, the parental UROtsa model showed decreases in the expression of GATA3, PPARγ, and XBP1. These results suggest the parental UROtsa spheroid and serial passages have increased expression of basal cells and invasion and disease progression.

Overall, the unique gene signatures found in the spheroids and serial passages compared to the original cell lines indicates the role that serum has on the ability to differentiate cells and the growth environment of cells directly influences the gene expression of those cells and their ability to differentiate into cells with unknown characteristics and properties.

ABBREVIATIONS

2D   Two-dimensional

3D   Three-dimensional

AP-1   Activator protein 1

As^{3+} Arsenite

As^{5+} Arsenate

ATP   Adenosine triphosphate

BER   Base excision repair

CCND1   Cyclin D1

Cd^{2+} Cadmium

CD24   Cluster of differentiation 24

CD44   Cluster of differentiation 44

$CdCl_2$ Cadmium chloride

CDH3   Cadherin 3

CYP2J2   Cytochrome P450 family 2 subfamily J member 2

DMA   Di-methylated

DMEM   Dulbecco's modified Eagle's medium

DNA   Deoxyribonucleic acid

EDTA   Ethylenediaminetetraacetic acid

ERBB2   Erb-β2 receptor tyrosine kinase 2

ERBB3   Erb-β2 receptor tyrosine kinase 3

FABP4   Fatty acid binding protein 4

FGFR3   Fibroblast growth factor receptor 3

FOXA1   Forkhead box A1

GATA3   GATA binding protein 3

GC   Gemcitabine plus cisplatin

GPX2   Glutathione peroxidase 2

GSH   Glutathione

H & E   Hematoxylin and eosin

HMOX1   Heme oxygenase 1

iAs   Inorganic arsenic

IEG   Intermediate early genes

IPA   Ingenutiy pathway analysis

I-κB   Inhibitor of κB

KPNA2   Karyopherin subunit alpha 2

KRT1   Keratin 1

KRT14   Keratin 14

KRT16   Keratin 16

KRT17   Keratin 17

KRT18   Keratin 18

KRT19   Keratin 19

KRT20   Keratin 20

KRT5   Keratin 5

KRT6A   Keratin 6A

KRT6B   Keratin 6B

KRT6C   Keratin 6C

KRT7   Keratin 7

KRT8   Keratin 8

MAPK   Mitogen-activated protein kinase

MDM2   MDM2 proto-oncogene

MIBC   Muscle-invasive bladder cancer

MMA   Mono-methylated

MMR   Mismatch repair

mRNA   Messenger RNA

MT   Metallothionein

mTOR   Mammalian target of rapamycin

MVAC   Methotrexate, vinblastine, doxorubicin, and cyclophosphamide

NaAsO$_2$ Sodium arsenate

NER   Nucleotide excision repair

NF-κB   nuclear factor kappa-light-chain-enhancer of activated B cells

PCA   Principle Component Analysis

PD-1   Programmed cell death protein

PD-L1/2   Programmed death ligand 1/2

PI3K   Phosphatidylinositol-3-kinase

PIK3CA	phosphatidylinositol-4,5-bisphosphate 3-kinase catalytic subunit alpha
PPARG	Peroxisome proliferator activated receptor gamma
PTEN	Phosphatidylinositol (3,4,5)-trisphosphate phosphatase and tensin homolog
RB	Retinoblastoma
RNA	Ribonucleic acid
ROS	Reactive oxygen species
RTK	Receptor tyrosine kinase
SCC	Squamous cell carnicoma
SV40	Polyomavirus simian virus 40
TP53	Tumor protein 53
TP63	Tumor protein 63
TURBT	Transurethral resection of the bladder tumor
UPK1B	Uroplakin 1B
UPK2	Uroplakin 2
UPK3	Uroplakin 3
XBP1	X-box binding protein 1

REFERENCES

Alishahi, S., Dyrne, D., Goodman, M., C., & Baxby, K. (2002, February). Haematuria investigation based on a standard protocol: emphasis on the diagnsis of urological malignancy. *Journal of the Royal College of Surgeons of Edinburgh, 47*(1), 422-427.

Antoni, S., Ferlay, J., Soerjomataram, I., Znaor, A., Jemal, A., & Bray, F. (2016, June 8). Bladder Cancer Incidence and Mortality: A Global Overview and Recent Trends. *European Association of Urology, 71*, 96-108.

Apodaca, G. (2004). The Urothelium: Not Just a Passive Barrier. *Traffic, 5*, 117-128.

Badalament, R. A., Fair, W. R., Whitemore Jr., W. F., & Melamed, M. R. (1988, February). The relative value of cytometry and cytology in the management of bladder cancer: the Memorial Sloan-Kettering Cancer Center experience. *Seminars in Urolgoy, 6*(1), 22-30.

Bakkar, A. A., Wallerand, H., Radvanyi, F., Lahaye, J.-B., Pissard, S., Lecerf, L., . . . Medina, D. d. (2003, December 1). FGFR3 and TP53 Gene Mutations Define Two Distinct Pathways in Urothelial Cell Carcinoma of the Bladder. *Cancer Research, 63*, 8,1018-8,112.

Beyersmann, D. (2002, February 28). Effects of carcinogenic metals on gene expression. *Toxicology Letters, 127*, 63-68.

Bos, J. L. (1989, September 1). ras Oncogenes in Human Cancer: A Reivew. *Cancer Research, 49*, 4,682-4,689.

Burger, M., Grossman, H. B., Droller, M., Schmidbauer, J., Hermann, G., Drăgoescu, O., . . . Jocham, D. (2013, November). Photodynamic Diagnosis of Non–muscle-invasive Bladder Cancer with Hexaminolevulinate Cystoscopy: A Meta-analysis of Detection and Recurrence Based on Raw Data. *European Urology, 64*(5), 846-865.

Calmette, A. (1927). La Vaccination Préventive Contre la Tuberculose par le "BCG". *Paris Masson, 79*, 79.

Cancer, I. A. (1980). *Monographs on the Evaluation of the Carcinogenic Risk of Chemicals to Man: Some Metals and Metallic Compounds* (Vol. 23).

Cancer, I. A. (1993). Cadmium and Cadmium Compounds. *Monograph*, 121-145.

Cancer, I. A. (2002). Arsenic and Arsenic Compounds. *Monograph*, 41-93.

Cappellen, D., De Oliveira, C., Ricol, D., Diez de Medine, S. G., Bourdin, J., Sastre-Garau, X., . . . Radvanyi, F. (1999, September). Frequent activating mutations of FGFR3 in human bladder and cervix carcinomas. *Nature Genetics, 23*, 18-20.

Chen, G. F., Shi, T. P., Wang, B. J., Wang, X. Y., & Q, Z. (2015). Efficacy of Different Resections of Non-Muscle-Invasive Bladder Cancer and Analysis of the Optimal Surgical Method. *Journal of Biological Regulators and Homeostatic Agents*, 465-470.

Cheng, L., Montironi, R., Davidson, D. D., & Lopez-Beltran, A. (2009). Staging and reporting of urothelial carcinoma of the urinary bladder. *Modern Pathology, 22*, S70-S95.

Chism, D. D. (2017, October). Urothelial Carcinoma of the Bladder and the Rise of Immunotherapy. *Journal of the National Comprehensive Cancer Network, 15*(10), 1,277-1,284.

Choi, W., Porten, S., Kim, S., Willis, D., Plimack, E. R., Hoffman-Censits, J., . . . Pretzsch, S. (2014, February 10). Identification of distinct basal and luminal subtypes of muscle-invasive bladder cancer with different sensitivities to frontline chemotherapy. *Cancer Cell, 25*(2), 152-165.

Clark, P. E., Spiess, P. E., Agarwal, N., Bangs, R., Boorjian, S. A., Buyyounouski, M. K., . . . Meeks, J. J. (2016, October). NCCN Guidelines Insights: Bladder Cancer, Version 2.2016. *Jouranl of the National Comprehensive Cancer Network, 14*(10), 1,213-1,224.

Cohen, S. M. (1998). Cell Proliferation and Carcinogenesis. *Drug Metabolism Reviews, 30*(2), 339-357.

Corporation, S. A. (1987). Estimated National Occurrence and Exposure to Arsenic in Public Drinking Water Supplies.

Costa, R. M., Chiganças, V., da Silva Galhardo, R., Carvalho, H., & Mench, C. F. (2003, November). The eukaryotic nucleotide excision repair pathway. *Biochimie, 85*(11), 1,083-1,099.

Crawford, J. M. (2008, July). The origins of bladder cancer. *Laboratory Investigation, 88*, 686-693.

Damrauer, J. S., Hoadley, K. A., Chism, D. D., Fan, C., Tiganelli, C. J., Wobker, S. E., . . . Kim, W. Y. (2014). Intrinsic subtypes of high-grade bladder cancer reflect the hallmarks of breast cancer biology. *Proceedings of the National Academy of Sciences of the United States of America, 111*(8), 3,110-3,115.

De Santis, M., Bellmunt, J., Mead, G., Kerst, J. M., Leahy, M., Maroto, P., . . . Sylvester, R. (2012, January 10). Randomized phase II/III trial assessing gemcitabine/carboplatin and methotrexate/carboplatin/vinblastine in patients with

advanced urothelial cancer who are unfit for cisplatin-based chemotherapy: EORTC study 30986. *Journal of Clinical Oncology, 30*(2), 191-199.

Delclos, G. L., & Lerner, S. P. (2008, September). Occupational risk factors. *Scandinavian Journal of Urology and Nephrology, 218*, 58-63.

Donat, S. M., Shabsigh, A., Savage, C., Cronin, A. M., Bochner, B. H., Dalbagni, G., . . . Milowsky, M. I. (2009, January). Potential Impact of Postoperative Early Complications on the Timing of Adjuvant Chemotherapy in Patients Undergoing Radical Cystectomy: A High-Volume Tertiary Cancer Center Experience. *European Urology, 55*(1), 177-186.

Drobna, Z., Styblo, M., & Thomas, D. J. (2009). An Overview of Arsenic Metabolism and Toxicity. *Current Protocols in Toxicology, 42*(431), 1-6.

Droller, M. J. (1998, September/October). Bladder Cancer: State-of-the-Art Care. *California Cancer Journal of Clinicians, 48*(5), 269-284.

Droller, M. J. (1998, February 1). Commentary on Sarodsy M F et al: Improved detection of recurrent bladder cancer using the bard BTA stat test. *The Journal of Urology, 159*(2), 601-602.

D'souza, N., & Verma, A. (2016, October-December). Holmium laser transurethral resection of bladder tumor: Our experience. *Urology Annuals, 8*(4), 439-443.

Elsebai, I. (1977, March/April). Parasites in the Etiology of Cancer - Bilharziasis and Bladder Cancer. *CA: A Cancer Journal for Clinicians, 27*(2), 100-106.

Ernst, P., & Theriault, G. (1984, April 1). Known occupational carcinogens and thier significance. *Canadian Medical Association Journal, 130*(7), 863-867.

Feki-Tounsi, M., Olmedo, P., Gil, F., Khlifi, R., Mhiri, M.-N., Rebai, A., & Hamza-Chaffai, A. (2013, October). Cadmium in blood of Tunisian men and risk of bladder cancer: interactions with arsenic exposure and smoking. *Environmental Science and Pollution Research, 20*(10), 7,204-7,213.

Feustel, A., & Wennrich, R. (1986). Zinc and cadmium plasma and erythrocyte levels in prostatic carcinoma, BPH, urological malignancies, and inflammations. *The Prostate, 8*(1), 75-79.

Furuse, H., & Ozono, S. (2010). Transurethral resection of the bladder tumor (TURBT) for non-muscle invasive bladder cancer: Basic skills. *International Journal of Urology, 17*, 698-699.

Galsky, M. D., Pal, S. K., Chowdhury, S., Harshman, L. C., Crabb, S. J., Wong, Y. N., . . . Vaishampayan, U. N. (2015, August 1). Comparative effectiveness of gemcitabine plus cisplatin versus methotrexate, vinblastine, doxorubicin, plus cisplatin as neoadjuvant therapy for muscle-invasive bladder cancer. *Cancer, 121*(15), 2,586-2,593.

Giaginis, C., Gatzidou, E., & Theocharis, S. (2006, March 21). DNA repair systems as targets of cadmium toxicity. *Toxicology and Applied Pharmacology, 213*, 282-290.

Goebell, P. J., & Knowles, M. A. (2010, July-August). Bladder cancer or bladder cancers? Genetically distinct malignant conditions of the urothelium. *Urologic Oncology, 4*, 409-428.

Goodrich, D. W., Wang, N. P., Yue-Wei, Q., Lee, E. T.-H., & Lee, W.-H. (1991, October 18). The retinoblastoma gene product regulates progression through the G1 phase of the cell cycle. *Cell, 67*(2), 293-302.

Gray, P. J., Fedewa, S. A., Shipley, W. U., Efstathiou, J. A., Lin, C. C., Zietman, A. L., & Virgo, K. S. (2013, May). Use of Potentially Curative Therapies for Muscle-invasive Bladder Cancer in the United States: Results from the National Cancer Data Base. *European Urology, 63*(5), 823-829.

Hayakawa, Toru, Kobayashi, Y., Cui, X., & Hirano, S. (2005, April). A new metabolic pathway of arsenite: arsenic–glutathione complexes are substrates for human arsenic methyltransferase Cyt19. *Archives of Toxicology, 79*(4), 183-191.

He, X., Marchionni, L., Hansel, D. E., Yu, W., Sood, A., Yang, J., . . . Berman, D. M. (2009, July). Differentiation of a Highly Tumorigenic Basal Cell Compartment in Urothelial Carcinoma. *Stem Cells, 27*(7), 1,487-1,495.

Heney, N. M., Ahmed, S., Flanagan, M. J., Frable, W., Corder, M. P., Hafermann, M. D., & Hawkins, I. R. (1983, December). Superficial Bladder Cancer: Progression and Recurrence. *The Journal of Urology, 130*(6), 1,083-1,086.

Herr, H. W. (2006, October). Max Nitze, the Cystoscope and Urology. *The Journal of Urology, 176*, 1,313-1,316.

Holbro, T., Beerli, R. R., Maurer, F., Koziczak, M., Barbas III, C. F., & Hynes, N. E. (2003, July 22). The ErbB2/ErbB3 heterodimer functions as an oncogenic unit: ErbB2 requires ErbB3 to drive breast tumor cell proliferation. *Proceedings of the National Academy of Sciences of the United States of America, 100*(15), 8,933-8,938.

Hopenhayn-Rich, C., Biggs, M. L., Fuchs, A., Bergoglio, R., Tello, E. E., Nicolli, H., & H, S. A. (1996, March). Bladder Cancer Mortality Associated with Arsenic in Drinking Water in Argentina. *Epidemiology, 7*(2), 117-124.Hsieh, P. (2001, July 12). Molecular mechanisms of DNA mismatch repair. *Mutation Research/DNA Repair, 486*(2), 71-8.

Humans, I. W. (2010). *IARC Monographs on the Evaluation of Carcinogenic Risks to Humans, No. 99.* Lyon, France.

Jackson, A. M., Alexandroff, A. B., Fleming, D., Prescott, S., Chisholm, G. D., & K, J. (1994, September). Bacillus-calmette-guerin (bcg) organisms directly alter the growth of bladder-tumor cells. *International Journal of Oncology, 5*(3), 697-703.

Johansson, S. L., & Cohen, S. M. (1998, December 7). Epidemiology and etiology of bladder cancer. *Seminars in Surgical Oncology, 13*(5), 1-30.

Joseph, P. (2009, August 1). Mechanisms of cadmium carcinogenesis. *Toxicological and Applied Pharmacology*(238), 272-279.

Kaghad, M., Bonnet, H., Yang, A., Creancier, L., Biscan, J.-C., Valent, A., . . . Caput, D. (1997, August 22). Monoallelically Expressed Gene Related to p53 at 1p36, a Region Frequently Deleted in Neuroblastoma and Other Human Cancers. *Cell, 90*(4), 809-819.

Kapahi, P., Takahashi, T., Natoli, G., Adams, S. R., Chen, Y., Tsien, R. Y., & Karin, M. (2000, November 17). Inhibition of NF-κB Activation by Arsenite through Reaction with a Critical Cysteine in the Activation Loop of IκB Kinase. *Journal of Biological Chemistry, 275*(46), 36,062-36,066.

Kavaler, E., Landman, J., Y, C., Droller, M. J., & Liu, B. C. (1998, February 15). Detecting human bladder carcinoma cells in voided urine samples by assaying for the presence of telomerase activity. *Cancer, 82*(4), 708-714.

Kellen, A., Zeegers, M. P., Hond, E. D., & Buntinx, F. (2007). Blood cadmium may be associated with bladder carcinogenesis: The Belgian case–control study on bladder cancer. *Cancer Detection and Prevention, 31*(1), 77-82.

Khadra, M. H., Pickard, R. S., Charlton, M., Powell, P. H., & Neal, D. E. (2000, February). A Prospective Analysis of 1,930 Patients with Hematuria to Evaluate Current Diagnostic Practice. *The Journal of Urology, 163*(2), 524-527.

Kitchin, K. T., & Wallace, K. (2008, March). The role of protein binding of trivalent arsenicals in arsenic carcinogenesis and toxicity. *Journal of Inorganic Biochemistry, 102*(3), 532-539.

Klaassen, C. D., Liu, J., & Choudhuri, S. (1999). Metallothionein: An intracellular protein to protect against cadmium toxicity. *Annual Review of Pharmacology and Toxicology, 39*, 267-294.

Lapham, R. L., Ro, J. Y., Staerkel, G. A., & Ayala, A. G. (1997, September/October). Pathology of transitional cell carcinoma of the bladder and its clinical implications. *Seminars in surgical oncology, 13*(5), 307-318.

Li, L., & Chen, F. (2016, April). Oxidative Stress, Epigenetics, and Cancer Stem Cells in Arsenic Carcinogenesis and Prevention. *Current Pharmacology Reports, 2*(2), 57-63.

Li, Y., Ishiguro, H., Kawahara, T., Kashiwai, E., Izumi, K., & Miyamoto, H. (2014, January). Loss of GATA3 in bladder cancer promotes cell migration and invasion. *Cancer Biology & Therapy, 15*(4), 428-435.

Lilyestrom, W., Klein, M. G., Zhang, R., Joachimiak, A., & Chen, X. (2006, September 1). Crystal structure of SV40 large T-antigen bound to p53: interplay between a viral oncoprotein and a cellular tumor suppressor. *Genes & Development, 20*(17), 2,373-2,382.

Lin, Y., Miyamoto, H., Fujinami, K., Uemura, H., Hosaka, M., Iwasaki, Y., & Kubota, Y. (1996, June). Telomerase activity in human bladder cancer. *Clinical Cancer Research, 2*, 929-932.

Lindgren, D., Frigyesi, A., Gudjonsson, S., Sjödahl, G., Hallden, C., Chebil, G., . . . Höglund, M. (2010). Combined gene expression and genomic profiling define two intrinsic molecular subtypes of urothelial carcinoma and gene signatures for molecular grading and outcome. *Cancer Research, 70*(9), 3,463-3,472.

Lotan, Y., & Roehrborn, C. G. (2003, February). Sensitivity and specificity of commonly available bladder tumor markers versus cytology: Results of a comprehensive literature review and meta-analyses. *Urolgoy, 61*(1), 109-118.

Lui, J., Qu, W., & Kadiiska, M. B. (2009, August 1). Role of oxidative stress in cadmium toxicity and carcinogenesis. *Toxicological and Applied Pharmacology, 238*(3), 209-214.

Maehama, T., & Dixon, J. E. (1998, May 29). The Tumor Suppressor, PTEN/MMAC1, Dephosphorylates the Lipid Second Messenger, Phosphatidylinositol 3,4,5-Trisphosphate. *The Journal of Biological Chemistry, 273*, 13,375-13,378.

Mah, V., & Jalilehvand, F. (2010). Cadmium(II) complex formation with glutathione. *Journal of Biological Inorganic Chemistry, 15*, 441-458.

Malats, N., & Real, F. X. (2015). Epidemiology of Bladder Cancer. *Hematology/Oncology Clinics of North America, 29*, 177-189.

Malkowicz, S. B., van Poppel, H., Mickisch, G., Pansadoro, V., Thüroff, J., Soloway, M. S., . . . Fukui, I. (2007). Muscle-invasive urothelial carcinoma of the bladder. *Urology, 69*, 3-16.

Malumbres, M., & Barbacid, M. (2003). RAS Oncogenes: the first 30 years. *Nature Reviews Cancer, 3*, 459-465.

Mandevilla, J. A., Neta, B. S., Vanni, A. J., L, S. G., Riger-Christ, K. M., Zeheb, R., . . . Summerhayes, I. C. (2008). P-cadherin as a prognostic indicator and a modulator of migratory behavior in bladder carcinoma cells. *BJU International, 102*(11), 1,707-1,714.

McConkey, D. J., Choi, W., Ochoa, A., & Dinney, C. P. (2016, October). Intrinsic subtypes and bladder cancer metastasis. *Asian Journal of Urology, 3*(4), 260-267.

Meliker, J. R., & Nriagu, J. O. (2007, November 1). Arsenic in drinking water and bladder cancer: review of epidemiological evidence. *Trace Metals and other Contaminants in the Environment, 9*, 551-584.

Meliker, J. R., Slotnick, M. J., AvRuskin, G. A., Schottenfled, D., Jacquez, G. M., Wilson, M. L., . . . Nriagu, J. O. (2010). Lifetime exposure to arsenic in drinking water and bladder cancer: a population-based case-control study in Michigan, USA. *Cancer Cause & Control*, 745-757.

Memisoglu, A., & Samson, L. (2000, June 30). Base excision repair in yeast and mammals. *Mutation Research/Fundamental and Molecular Mechanisms of Mutagenesis, 451*(1-2), 39-51.

Metts, M. C., Metts, J. C., Milito, S. J., & Thomas Jr., C. R. (2000, June). Bladder Cancer: A Review of Diagnosis and Management. *Journal of the National Medical Assocation, 92*(6), 285-294.

Morales, A., Eidinger, D., & Bruce, A. W. (1976, August). Intracavitary Bacillus Calmette-guerin in the Treatment of Superficial Bladder Tumors. *The Journal of Urology, 116*(2), 180-182.

Naiki, T., Naiki-Ito, A., Etani, T., Iida, K., Ando, R., Nagai, T., . . . Yasui, T. (2017, May 16). GPX2 is a Prognostic Marker and has a Therapeutic Potential via Regulation of Oxidative Stress in Bladder Cancer. *The Journal of Urology, 197*(4S), e1316.

Ornitz, D. M. (2001). Fibroblast Growth Factors: Evolution. *Genome Biology, 12*, 1-12.

Overley-Adamson, B., Artlett, C. M., Stephens, C., Sassi-Gaha, S., Weis, R. D., & Thacker, J. D. (2014). Targeting the unfolded protein response, XBP1, and the NLRP3 inflammasome in fibrosis and cancer. *Cancer Biology & Therapy, 15*(4), 452-462.

Pelucchi, C., & La Vecchia, C. (2009, February). Alcohol, coffee, and bladder cancer risk: a review of epidemiological studies. *European Journal of Cancer Prevention, 18*(1), 62-68.

Perou, C. M., Sørlie, T., Eisen, M. B., van de Rijn, M., Jeffrey, S. S., Rees, C. A., . . . Williams, C. (2000). Molecular portraits of human breast tumours. *Nature, 406*, 747-752.

Petzoldt, J. L., Leigh, I. M., Duffy, P. G., Sexton, C., & Masters, J. R. (1995). Immortalisation of human urothelial cells. *Urological Research, 23*, 377-380.

Przybojewska, B., Jagiello, A., & Jalmuzna, P. (2000, August). H-RAS, K-RAS, and N-RAS Gene Activation in Human Bladder Cancers. *Cancer Genetics and Cytogenetics, 121*(1), 73-77.

Puzio-Kuter, A. M., Castillo-Martin, M., Kinkade, C. W., Wang, X., Shen, T. H., matos, T., . . . Abate-Shen, C. (2009). Inactivation of p53 and Pten promotes invasive bladder cancer. *Genes & Development, 23*, 675-680.

Redelman-Sidi, G., Glickman, M. S., & Bochner, B. H. (2014). The mechanism of action of BCG therapy for bladder cancer—a current perspective. *Nature Reviews Urology, 11*, 153-162.

Reedman, N. D., Silverman, D. T., Hollenbeck, A. R., Schatzkin, A., & Abnet, C. C. (2011, August 17). Association Between Smoking and Risk of Bladder Cancer Among Men and Women. *Journal of the American Medical Association, 306*(7), 737-745.

Registry, A. f. (2012). Toxicological Profile for Cadmium. *US Department of Health and Human Services*.

Reya, T., Morrison, S. J., Clarke, M. F., & Weissman, I. L. (2001, November 1). Stem cells, cancer, and cancer stem cells. *Nature, 414*, 105-111.

Rhijn, a., G, B. W., van der Kwast, T. H., Vis, A. N., Kirkels, W. J., Boevé, E. R., . . . Zwarthoff, E. C. (2004, March 15). FGFR3 and P53 Characterize Alternative Genetic Pathways in the Pathogenesis of Urothelial Cell Carcinoma. *Cancer Research, 64*, 1,911-1914.

Rieger-Christ, K. M., Mourtzinos, A., Lee, P. J., Zagha, R. M., Cain, J., Silverman, M., . . . Summerhayes, I. C. (2003, August 15). Identification of fibroblast growth factor receptor 3 mutations in urine sediment DNA samples complements cytology in bladder tumor detection. *Cancer, 98*(4), 737-744.

Rossi, M. R., Masters, J. R., Park, S., Todd, J. H., Garrett, S. H., Sens, M. A., . . . Sens, D. A. (2001, August). The Immortalized UROtsa Cell Line as a Potential Cell Culture Model of Human Urothelium. *Environmental Health Perspectives, 109*(8), 801-808.

Saluja, M., & Gilling, P. (2018). Intravesical bacillus Calmette-Guérin instillation in non-muscle-invasive bladder cancer: A review. *International Journal of Urology, 25*, 18-24.

Sarodsy, M. F., Hudson, M. A., Ellis, W. J., Soloway, M. S., deVere White, R., Sheinfeld, J., . . . Pfalzgraf, R. D. (1997, September). Improved detection of recurrent bladder cancer using the bard bta stat test. *Urology, 50*(3), 349-353.

Satarug, S., Baker, J. R., Urbenjapol, S., Haswell-Elkins, M., Reilly, P. E., Williams, D. J., & Moore, M. R. (2005). A global perspective on cadmium pollution and toxicity in non-occupationally exposed population. *Toxicology Letters, 137*, 65-83.

Schmidt, C. W. (2015, January). In Search of "Just Right": The Challenge of Regulating Arsenic in Rice. *Environmental Health Prospective, 123*(1), 16-19.

Sens, D. A., Park, S., Gurel, V., Sens, M. A., Garrett, S. H., & Somji, S. (2004, May 1). Inorganic Cadmium- and Arsenite-Induced Malignant Transformation of Human Bladder Urothelial Cells. *Toxicological Sciences, 79*(1), 56-63.

Shirodkar, S. P., & Lokeshwar, V. B. (2009, September). Potential New Markers in the Early Detection of Bladder Cancer. *Current Opinions in Urology, 19*(5), 488-495.

Shuman, L., Zheng, Z., Yamashita, H., Warrick, J., Kaestner, K., & DeGraff, D. (2017, May 16). FOXA1 Knockout is Associated with Increased Carcinogenic Susceptibility and Androgen Receptor Expression in Murine Bladder Cancer. *The Journal of Urology, 197*(4S), e1316.

Siemiatycki, J., Dewar, R., Nadon, L., & Gérin, M. (1994, December 15). Occupational risk factors for bladder cancer: results from a case-control study in Montreal, Quebec, Canada. *American Journal of Epidemiology, 140*(12), 1,061-1,080.

Singh, S. K., Clarke, I. D., Terasaki, M., Bonn, V. E., Hawkins, C., Squire, J., & Dirks, P. B. (2003, September 15). Identification of a Cancer Stem Cell in Human Brain Tumors. *Cell and Tumor Biology, 63*, 5,821-5,828.

Sjödahl, G., Lauss, M., Lövgren, K., Chebil, G., Gudjonsson, S., Veerla, S., . . . Höglund, M. (2012, June 15). A Molecular Taxonomy for Urothelial Carcinoma. *Clinical Cancer Research, 18*(12), 3,377-3,386.

Skinner, D. G., & Lieskovsky, G. (1984, June). Contemporary Cystectomy with Pelvic Node Dissection Compared to Preoperative Radiation Therapy Plus Cystectomy in Management of Invasive Bladder Cancer. *The Journal of Urology, 131*(6), 1,069-1,072.

Smith, A. H., Goycolea, M., Haque, R., & Biggs, M. L. (1998, April 1). Marked increase in bladder and lung cancer mortality in a region of Northern Chile due to arsenic in drinking water. *American Journal of Epidemiology, 147*(7), 660-669.

Smith, A. H., Hopenhayn-Rich, C., Bates, M. N., Goeden, H. M., Hertz-Picciotto, I., Duggan, H. M., . . . Smith, M. T. (1992). Cancer Risks from Arsenic in Drinking Water. *Environmental Health Perspective, 97*, 259-267.

Sridhar, S. S. (2017, May). Evolving Treatments of Advanced Urothelial Cancer. *American Society of Clinical Oncology, 13*(5), 309-316.

Staack, A., Koenig, F., Daniltchenko, D., Hauptmann, S., Loening, S. A., Schnorr, D., & Jung, K. (2002, February). Cathepsins B, H, and L activities in urine of patients with transitional cell carcinoma of the bladder. *Urology, 59*(2), 308-312.

Steinberg, R. L., Thomas, L. J., & Nepple, K. G. (2016, June). Intravesical and alternative bladder-preservation therapies in the management of non–muscle-

invasive bladder cancer unresponsive to bacillus Calmette-Guérin. *Urologic Oncology, 34*(6), 279-289.

Thomas, D. J., Styblo, M., & Lin, S. (2001, October 15). The Cellular Metabolism and Systemic Toxicity of Arsenic. *Toxicology and Applied Pharmacology, 176*(2), 127-144.

Tumeh, P. C., Harview, C. L., Yearley, J. H., Shintaku, P., Taylor, E. J., Robert, L., . . . Spasic, M. (2014, November). PD-1 blockade induces responses by inhibiting. *Nature, 515*, 568-571.

van der Meijden, A. P. (1998). Bladder Cancer. *The BMJ, 317*, 1,366-1,369.

Wai, C. Y., & Miller, D. S. (2002, September). Urinary Bladder Cancer. *Clinical Obstetrics and Gynecology, 45*(3), 844-854.

Waisberg, M., Joseph, P., Hale, B., & Beyersmann, D. (2003, November 5). Molecular and cellular mechanisms of cadmium carcinogenesis. *Toxicology, 192*(2-3), 95-117.

Wei, J., Zaika, E., & Zaika, A. (2011, July 4). p53 Family: Role of Protein Isoforms in Human Cancer. *Journal of Nucleic Acids, 2012*, 1-19.

Witjes, J. A., Compérat, E., Cowan, N. C., De Santis, M., Gakis, G., Lebrét, T., . . . Riba, M. J. (2016). EAU Guidelines on Muscle-invasive and Metastatic Bladder Cancer. *Journal of Clinical Oncology, 34*, 1,945-1,952.

Yeung, C., Dinh, T., & Lee, J. (2014). The Health Economics of Bladder Cancer: An Updated Review of the Published Literature. *PharmacoEconomics, 32*, 1,093-1,104.

Yousef, P. G., & Gabril, M. Y. (2017, November 3). An update on the molecular pathology of urinary bladder tumors. *Pathology - Research and Practice, 214*, 1-6.

Zhang, Z.-T., Pak, J., Huang, H.-Y., Shapiro, E., Sun, T.-T., Pellicer, A., & Wu, X.-R. (2001). Role of Ha-ras activation in superficial papillary pathway of urothelial tumor formation. *Oncogene, 20*, 1,973-1,980.

Zhang, Z.-T., Pak, J., Shapiro, E., Sun, T.-T., & Wu, X.-R. (1999, July 15). Urothelium-specific Expression of an Oncogene in Transgenic Mice Induced the Formation of Carcinoma in Situ and Invasive Transitional Cell Carcinoma. *Cancer Research, 99*, 3,512-3,517.